Microphysical Properties of Three Types of Snow Clouds: Implication to Satellite Snowfall Retrievals

Hwayoung Jeoung[1], Guosheng Liu[1], Kwonil Kim[2], Gyuwon Lee[2], and Eun-Kyoung Seo[3]

1. Department of Earth, Ocean and Atmospheric Science, Florida State University, Tallahassee, Florida, U.S.A.
2. Department of Astronomy and Atmospheric Sciences, Center for Atmospheric REmote Sensing (CARE), Kyungpook National University, Daegu 41566, Republic of Korea
3. Department of Earth Science Education, Kongju National University, Kongju 314-701, Republic of Korea

Submitted to ACP, ICE-POP Special Issue (revised October 2020)

Abstract

Ground-based radar and radiometer data observed during the 2017-18 winter season over Pyeongchang area in the east coast of the Korean Peninsula were used to simultaneously estimate both cloud liquid water path and snowfall rate for three types of snowing clouds: near-surface, shallow and deep. Surveying all the observed data, it is found that near-surface cloud is the most frequently observed cloud type with an area fraction of over 60%, while deep cloud contributes the most in snowfall volume with about 50% of the total. The probability distributions of snowfall rates are clearly different among the three types of clouds, with vast majority hardly reaching to 0.3 mm h^{-1} (liquid water equivalent snowfall rate) for near-surface, 0.5 mm h^{-1} for shallow, and 1 mm h^{-1} for deep clouds. However, liquid water path in the three types of clouds all has substantial probability to reach 500 g m^{-2}. There is no clear correlation found between snowfall rate and liquid water path for any of the cloud types. Based on all observed snow profiles, brightness temperatures at Global Precipitation Measurement Microwave Imager channels are simulated, and the ability of a Bayesian algorithm to retrieve snowfall rate is examined using half the profiles as observations and the other half as *a priori* database. Under idealized scenario, i.e., without considering the uncertainties caused by surface emissivity, ice particle size distribution and particle shape, the study found that the correlation as expressed by R^2 between the "retrieved" and "observed" snowfall rates is about 0.32, 0.41 and 0.62, respectively, for near-surface, shallow and deep snowing clouds over land surface; these numbers basically indicate the upper limits capped by cloud natural variability, to which the retrieval skill of a Bayesian retrieval algorithm can reach. A hypothetical retrieval for the same clouds but over ocean is also studied, and a major improvement in skills is found for near-surface clouds with R^2 increased from 0.32 to 0.52, while smaller improvement is found for shallow and deep clouds. This study provides a general picture of the microphysical characteristics of the different types of snowing clouds and points out the associated challenges in retrieving their snowfall rate from passive microwave observations.

1. Introduction

Snowfall is an important component in the global hydrological cycle. Its global distribution may be observed using satellite-based passive and active microwave sensors. Currently, there are multiple satellites in operation carrying passive microwave sensors that are potentially able to be used for snowfall observations, which offers great spatial and temporal coverages for various snowfall related studies. Meanwhile, while only a few spaceborne active sensors are currently available for snowfall observations, they have the advantage of providing information on the vertical structure of precipitation. Nevertheless, whether active or passive sensors are used, in order to convert the observed radiative signatures (brightness temperature or radar reflectivity) to snowfall rate, two factors related to the snowing clouds play an essential role: one is the vertical extent of the cloud layer and the other is the cloud microphysical properties such as particles' phase and amount. Using ground-based observations from multiple sensors, in this study we intend to understand these properties for three distinctive types of snowing clouds. By performing radiative transfer simulations, we further investigate the implication of the variability in microphysical properties to satellite snowfall retrievals from passive microwave observations.

Snowfall retrieval has been investigated recently for both active and passive satellite measurements. The cloud radar onboard CloudSat satellite (Stephens et al., 2002; Tanelli et al., 2008) is the first spaceborne active sensor in operation that is suitable for snowfall observations. It has a minimum detectability of near −30 dBZ near the ground, allowing to observe the weak scattering signal from snowflakes. Kulie et al. (2016) used CloudSat cloud classification and snowfall rate retrievals to partition snowfall observations into shallow cumuliform and deep nimbostratus snowfall categories. Their results show that there are abundant shallow snow cloud cells globally and they can be associated with strong convection and heavy snowfall. For example, they found that shallow snowfall comprises about 36% in the 2006–10 CloudSat snowfall dataset by occurrence, while constituting some 18% of the estimated annual global snowfall accumulation. Shallow precipitation can be easily missed by space-borne radars. Although CloudSat radar provides information on the vertical structure of precipitation, there is a blind zone below about 1.5 km due to ground clutter contamination. In most analysis, the lowest range bin (bin depth is ~240 m) where radar data are not contaminated by surface clutter is often the third (fifth) above the actual surface over oceanic (land) surfaces (Wood et al., 2013; Kulie and Bennartz, 2009; Liu, 2008a; Marchand et al., 2008). Hudak et al.(2008) studied the ability of CloudSat radar to detect precipitation in cold season clouds using data from a C band weather radar at King City, Ontario. They found that the most frequent cause of a miss in detection by CloudSat radar was due to ground clutter removal of valid echoes by the algorithm. Similarly, Chen et al. (2016) compared snowfall estimates from CloudSat radar (Wood et al., 2013) and ground radar derived Multi-Radar and Multi-Sensor (MRMS) product (Zhang et al., 2016), and found that the lowest height with valid estimate for most (99.41%) snowfall events in CloudSat product is over 1 km above surface, whereas it for 76.41% of the corresponding MRMS observations is below 1 km.

Using satellite passive microwave observations at high frequency channels, snowfall may be retrieved due to the scattering of upwelling radiation by snowflakes (Katsumata et al., 2000; Bennartz and Bauer, 2003; Skofronick-Jackson and Johnson, 2011; Gong and Wu, 2017). Retrieval algorithms have been developed both in research mode (Kim et al., 2008; Kongoli et al., 2015; Liu and Seo, 2013; Noh et al., 2006; Skofronick-Jackson et al., 2004) and for operations (Kummerow et al., 2015; Meng et al., 2017). Skofronick-Jackson et al. (2004) and Kim et al. (2008) developed physically-based retrieval algorithms which seek the best match between radiative transfer model simulated and satellite observed brightness temperatures. The Liu and Seo (2013) and Kongoli et al. (2015) algorithms are mostly statistical in which many pairs of radar and/or gauge-measured snowfall and satellite measured brightness temperatures are used to develop their statistical relations. The Noh et al. (2006) and Kummerow et al. (2015) snowfall algorithms are based on the Bayesian theorem; an *a priori* database linking snowfall and brightness temperatures needs to be prepared before conducting retrievals. The snowfall rates in a Bayesian algorithm database are often retrievals from radars and the brightness temperatures are either those collocated measurements of passive microwave radiometers or simulated by radiative transfer models. The Meng et al. (2017) algorithm uses a one-dimensional variational method to seek the consistency between measured brightness temperatures and microphysical properties in the atmospheric column. Its performance has been verified by surface radar and gauge observations over the U.S. with satisfactory results.

Although the above successes have been achieved by previous investigators, there are still large discrepancies among different snowfall retrievals (Casella et al., 2017; Skofronick-Jackson et al., 2017; Tang et al., 2017). Algorithm uncertainty arises from many factors; one of them is the insufficient knowledge of microphysical properties of the snowing clouds, in particular, the amount of cloud liquid water. The increase in brightness temperature over cloudy skies due to liquid water emission in snowing clouds complicates the snowfall detection and retrieval problems (Liu and Curry, 1997; Liu and Seo, 2013; Wang et al., 2013). Wang et al. (2013) showed that the warming by liquid water emission has a similar magnitude to the cooling by ice scattering on microwave brightness temperatures at frequencies higher than 80 GHz. Liu and Seo (2013) discovered a warming rather than cooling signal in high-frequency brightness temperature in most snowfall cases they analyzed.

In addition, correctly simulating brightness temperatures is needed for physical snowfall retrievals as well as data assimilation of radiance observations in numerical weather prediction models. Yin and Liu (2019) has studied the bias characteristics of observed minus simulated brightness temperatures at high frequency channels of Global Precipitation Measurement Microwave Imager (GPM/GMI) under snowfall conditions. In their study, a radiative transfer model that includes single-scattering properties of non-spherical snow particles is used to simulate brightness temperatures at 89 through 183 GHz. The input snow water content profiles are derived from CloudSat radar measurements. The results show that the discrepancy between simulated and observed brightness temperatures is the greatest for very shallow (cloud top around 2 km) or very deep (cloud top around 8 km) snowing clouds with discrepancy value being over 10 K in the former and over 30 K in the latter case, although it is generally less than 3 K when averaged over all selected pixels under snowfall conditions. They explained the results as follows. For very shallow snowing clouds, cloud liquid water may be rich and contributes substantially to the observed brightness temperatures. However, the radiative transfer model, which uses CloudSat radar and GMI retrievals as input, failed to account for this liquid water abundance, resulting in a large discrepancy between simulated and observed brightness temperatures. For very deep snowing clouds, they hypothesized that CloudSat radar experiences substantial attenuation as well as non-Rayleigh scattering, which leads to higher simulated brightness temperatures than observed. A better understanding of the microphysical properties in very shallow and very deep snowing clouds is clearly needed to reduce the discrepancies between simulated and observed brightness temperatures.

A field experiment was conducted over the Korean Peninsula during the winter of 2017-2018, coinciding with the 2018 winter Olympic Games (ICE-POP 2018: International Collaborative Experiments for PyeongChang 2018 Olympic and Paralympic Winter Games). The experiment focuses on the measurement, physics, and improved prediction of heavy orographic snow in the Pyeongchang region of South Korea (Gehring et al., 2020). During the field experiment, many ground-based observations including radar, radiometer and *in situ* observations were conducted. In this study, we analyze the vertical structure and microphysical properties of these snowing clouds, with focus on their potential impacts on satellite remote sensing of snow precipitation. The main objective of the study is to gain better understanding of the characteristics of snowing clouds that are critical to satellite remote sensing of snowfall. Furthermore, we examine how a Bayesian snowfall retrieval algorithm with GPM/GMI observations would perform for the snowing clouds observed during this field experiment.

2. Data and Methods

2.1 Ground-based Cloud Radar and Radiometer

Observations from the Radiometer Physics GmbH-Frequency Modulated Continuous Wave 94 GHz cloud radar (RPG-FMCW, 2015) are the primary data source for this study. This vertical pointing radar is installed at 37.66°N, 128.70°E (altitude 735 m above sea level) over Korean Peninsula during the ICE-POP 2018 field campaign. It has an operation frequency of 94 GHz for radar backscatter and Doppler spectrum measurement and an embedded 89 GHz passive channel for liquid water path measurement. It is noted that while we refer this instrument as a cloud radar for convenience, it indeed includes an independent passive microwave channel at 89 GHz, which is used for cloud liquid water estimation. There is clearly an advantage of this instrument in studying the composition of cloud liquid and ice over those that measure radar reflectivity and brightness temperature by two separate instruments because this instrument measures emission and scattering signatures from the same cloud volume, therefore, avoids beam mismatching problem by a separated radar and radiometer. The vertical resolution of radar reflectivity measurement is selectable from 1, 5, 10, or 30 m, with overall radar calibration accuracy better than 0.4 dB. The minimum detectable radar reflectivity depends on the range and vertical resolution; at its typical operation mode of 30 m resolution, it is -36 dBZ at 10 km height, which is sufficiently sensitive for snowfall detection. In addition to radar reflectivity, the RPG-FMCW also measures Doppler spectrum with a Doppler velocity resolution of 1.5 cm s^{-1}. A detailed explanation of the calibration of this instrument can be found in Küchler et al. (2017).

2.2 Retrieved Microphysical Variables

In this study, the radar reflectivity Z_e is converted to snow water content (SWC) and snowfall rate (S) using the Z_e-SWC relation of Yin and Liu (2017) and Ze-S relation of Liu (2008a). Before performing these conversions, radar reflectivity was corrected for attenuation due to absorption by atmospheric gases and cloud liquid water, and scattering by ice particles. Absorption by atmospheric gases is calculated based on Rosenkranz (1998) for water vapor and Schwartz (1998) for oxygen with input of geophysical parameters interpolated from the Modern Era Reanalysis for Research and Applications Version-2 (MERRA-2) (Gelaro et al., 2017). Absorption by cloud liquid water is computed using liquid water path derived by the method described later in this section and assuming cloud liquid water uniformly distributed vertically in the radar echo layer. Refractive index of liquid water is calculated based on Liebe et al. (1993). Attenuation due to ice scattering was readily performed by manufacture-provided processing software (RPG-FMCW, 2015).

The Yin and Liu (2017) Z_e-SWC relation is given by

$$SWC = 0.024 Z_e^{0.75}, \tag{1}$$

where SWC is in g m^{-3} and Z_e is in mm^6 m^{-3}. In developing the above equation, three snow particle types are employed: sectors, dendrites (Liu, 2008b), and oblate aggregates (Honeyager et al., 2016). The backscatter cross sections of the three snowflake types are computed using discrete dipole approximation (DDA) (Draine and Flatau, 1994; Liu, 2004). It should be mentioned that although Eq.(1) is developed for CloudSat radar which has the same frequency as the RPG-FMCW radar, uncertainties in particle shapes and size distributions will certainly cause errors in snow water content derived in this study.

The Liu (2008a) S-Z_e relation is given by

$$Z_e = 11.5S^{1.25}, \tag{2}$$

where S is in mm h^{-1} (liquid water equivalent snowfall rate) and Z_e is in mm^6 m^{-3}. The backscatter cross sections in Eq.(2) are computed for rosettes, sectors and dendrites using DDA (Liu, 2008b).

In addition to radar reflectivity, the mean Doppler velocity and spectral width, the RPG-FMCW also measures brightness temperature at 89 GHz. While there is a liquid water path (LWP) variable produced by the manufacture-provided software, details about the liquid water path retrieval algorithm and its accuracy have not been well documented. In this study, we chose to adapt the algorithm of Liu and Takeda (1988) in computing liquid water path from 89 GHz brightness temperatures. Briefly, the brightness temperature T_B received by an up-looking radiometer can be divided into two portions, i.e., the cloud-free atmospheric emission and the liquid cloud water emission. The emissivity of the liquid water cloud ε_c may then be approximated by

$$\varepsilon_c = \frac{T_a(T_B - T_{Ba})}{T_c(T_a - T_{Ba})}, \tag{3}$$

where T_a is a radiatively-mean temperature of the atmosphere in Kelvin, which can be evaluated by absorption-coefficient-weighted averaging atmospheric temperatures in vertical. Its value roughly equals to the temperature around 1.5 km altitude. T_c is the mean temperature of the cloud layer, which is determined in this study by the air temperature at the height of the geometric middle of valid radar reflectivity profiles. T_{Ba} is the brightness temperature from the liquid-free atmosphere, which is derived using interpolation between measured T_Bs at echo-free regions in this study. From ε_c calculated from (3), liquid water path (LWP) can be derived by

$$\text{LWP} = \frac{\lambda \rho_L}{6\pi \Im\left\{\frac{m^2-1}{m^2+2}\right\}} ln\ (1 - \varepsilon_c)\ , \tag{4}$$

where m is the refractive index of water at temperature T_c, λ is wavelength, ρ_L is liquid water density (1000 kg m^{-3}) and $\Im\{\ \}$ indicates taking the imaginary part. In this study, the refractive index of liquid water is calculated based on Liebe et al. (1993). It should be cautioned that the refractive index at high microwave frequencies may not be very accurate for supercooled liquid water as pointed by Kneifel et al. (2014), which can result in errors in the liquid water path estimation. Another error in the liquid water path estimation can be caused by the omission of the reflection by snow particles to the upwelling radiation originated from surface emission in the retrieval algorithm. Based on estimation by Kneifel et al. (2010), this reflection can enhance downward radiation by 5 K at 89 GHz where heavy snow cloud occurs. The formulation of the current liquid water path retrieval algorithm has the advantage of using cloud-free observations (T_{Ba} in Eq.3) as background to calculate cloud emissivity, which is particularly useful when water vapor observations are lacking. However, the drawback is that it cannot include the contribution by ice scattering.

In Fig.1 shown is an example of the liquid water path retrieved in this study together with radar reflectivity cross sections and liquid water path retrieval from the manufacture-provided algorithm. It is seen that in cloud-free regions our liquid water path retrievals are close to zero, while the manufacture-provided retrievals have a positive bias of about 30 g m^{-2}. In cloudy regions, the two liquid water path values compare much closer to each other. Based on this comparison, we believe that the liquid water path values retrieved in this study are more reasonable. Therefore, our retrievals will be used in the following analysis.

2.3 Snowing Cloud Detection

All snow events have been identified from the RPG-FMCW observations during 1 November 2017 through 30 April 2018 (6 months). To separate snow and rain at surface, the scheme of Sims and Liu (2015) is implemented. In their study, the effects of multiple geophysical parameters on precipitation phase were investigated using global surface-based observations over multiple years. They showed that wet-bulb temperature is a key parameter for separating solid and liquid precipitation and the low-level temperature lapse rate also affects the precipitation phase. Geophysical parameters from MERRA-2 reanalysis (Gelaro et al., 2017) were used in this study as input to the Sims and Liu (2015) scheme. In addition, we use the near-surface reflectivity higher than -20 dBZ as the criterion for snowfall detection; all radar data analyzed for snowing clouds in the following sections have a near-surface radar reflectivity greater than -20 dBZ. In a study by Wang et al. (2017) based on CloudSat radar reflectivity profiles, they found that precipitation onset often occurs when radar reflectivity is about -18 to -13 dBZ. We use the value of -20 dBZ as criterion in this study to make sure that all possible snowfall cases are included in the precipitation samples.

Cloud top height is used for the determination of cloud types. As shown in Fig.2, radar reflectivity above cloud top is often noisy as shown between 11 and 16 UTC. Therefore, it is often problematic to determine cloud top height by simply using a radar reflectivity threshold. However, we found that Doppler spectral width is a reliable indicator to identify clouds as shown in the bottom panel in Fig.2. Using visual examination of this and some other cases, we found that Doppler spectral width commonly reduces to less than 0.1 m s^{-1} above cloud top. In Fig. 2, we show in the upper panel the cloud top height in the black solid line as determined by the criterion of the spectral width >0.1 m s^{-1} for snowing clouds with near-surface radar reflectivity greater than –20 dBZ. It appears that the criterion well captures the cloud tops.

2.4 Other Ancillary Data

While quantitative analysis was not conducted, data collected at the same location by PARticle SIze VELocity (PARSIVEL; Löffler-Mang and Joss, 2000; Battaglia et al., 2010; Tokay et al., 2014), 2-Dimensional Video Distrometer (2DVD; Kruger and Krajewski, 2002), and Multi-Angle Snowflake Camera (MASC; Garrett et al., 2012; Grazioli et al., 2017) are used for confirmation of precipitation phase and particle types. A PARSIVEL is an optical disdrometer which uses a 54 cm^2 laser beam in the wavelength of 650 nm. It measures the size and fall velocity of individual precipitation particles with diameter ranging from 0.2 mm to 25 mm for solid particles. An autonomous PARSIVEL unit (Chen et al., 2017) from NASA was collocated with the RPG-FMCW cloud radar during the field campaign. A collocated 2DVD provides detailed information on size, fall velocity, and shape of individual hydrometeors with two orthogonal fast line-scan cameras. The camera provides images of particles which are matched for individual particles. The matched individual particles are then corrected for shape distortion. In addition, detail images of particles are provided from MASC that is composed of three cameras separated horizontally by an angle of 36 degrees and simultaneously takes high-resolution (35 µm per pixel) photographs of free-falling hydrometeors. Hydrometeor classification algorithm based on the supervised machine learning technique (Praz et al., 2017) is applied to the individual images of particles. This procedure identified the precipitation type (small particles, columnar crystals, planer crystals, combination of columnar and plate crystals, aggregates, and graupel) and the degree of riming.

2.5 Dividing Snowing Clouds to Three Types

There are several synoptic weather patterns that cause snowfall over the Pyeongchang area. The first pattern is a synoptic low pressure system, so-called “cold low”, developed over the Yellow sea (west of Korea) or cold continent and causes the snowfall over the northern or middle part of Korea when moving to east (Chung et al. 2006; Ko et al. 2016; Park et al. 2019). As this system crosses the Korean peninsula, the system become weaker and shallower once moving over the Pyeongchang area. The precipitation intensity and depth of system depend on the strength of low pressure. The second synoptic pattern, “warm low,” develops over the warm ocean near East China sea or South sea and moves to north-east or east (Nam et al. 2014; Gehring et al 2020). This synoptic pattern brings abundant moisture to Korean Peninsula and is typically favored for vertically well-developed precipitation system. As the warm low pressure passes the Korean Peninsula and East sea, the winds over the Pyeongchang area and East sea turns to easterly or north-easterly, bringing in cold air to the east coastal area. Thus, we expect that the depth of precipitation system is likely first deep with large moisture and later becomes shallower as influenced by north-easterly cold air. The third interesting pattern, so-called “air-sea interaction”, is developed by the easterly or north-easterly flow due to the Kaema high over the northern mountain complex or high pressure over Manchuria by the eastward expansion of the Siberian high (Kim and Jin 2016; Kim el at 2019). Thus, the cold north-easterly or easterly flow enhances the interaction with warm moisture ocean, resulting in the development of shallow convection and thermal inversion in the lower troposphere. The shallow convective clouds move to the coastal and mountain area where they are lifted by the orography.

An example of radar reflectivity cross section is shown in Fig.1 where deeper clouds lead to shallower convective cells. This is the case of the second synoptic type, warm low. During the passage of the warm low, the system reached to 9 km. However, the precipitation system is shallower than 1 km during easterly or north-easterly flow when the warm low pressure passed the East sea. In consideration of the implications to satellite snowfall remote sensing, we group the snowing clouds into three types: deep, shallow and near-surface. The “deep” snowing clouds are those with cloud top higher than 4 km, which are considered to be easily detected by both space-borne radars and radiometers at high microwave frequencies. They are mostly generated by large-scale lifting of frontal systems. We define the “shallow” snowing clouds as those with cloud top between 1.5 and 4 km. Large part of the snowing clouds in this group are associated with convective cells in unstable airmasses after the passing of fronts. These are the group that space-radars and radiometers may sometimes have difficulties to detect because of their shallowness and liquid-water rich. The “near-surface” group is defined as those having cloud top lower than 1.5 km. Similar to the case of shallow snow clouds, the near-surface snow clouds also mostly occur after low pressure passing or during north-easterly/easterly flow, and are convective in nature. Because of their shallowness, this group of snowing clouds will likely be hidden within ground-clutters for space-radars. Ground-based observations have the advantage to detect them from bottom up.

In Fig.1, examples are shown for the three snowing cloud types, together with liquid water path retrieved from RPG-FMCW observations using algorithms described in section 2.2. In this case, the largest value of liquid water path was seen in the transition from shallow to near-surface snowing clouds near 12 UTC, while the strongest radar reflectivity values (i.e., the heaviest snowfall) occurred in the deep snowing cloud between 01 to 05 UTC on 24 December 2017.

Surveying all observed data for the entire winter, approximately 374 hours of observations are deemed as snowfall events after we apply the -20 dBZ threshold at the lowest bin and the Sims and Liu (2015) algorithm to exclude rain events. These observations are then averaged over each 5-minute interval to form 4491 samples. The relative frequencies of occurrence (area fraction, calculated by the number of samples of a given snow type divided by the total number of snowfall samples) and snowfall amount (volume fraction, calculated by the snowfall amount produced by a given snow type divided by the total snowfall amount by all types) for the three types of snowing clouds are shown in Fig.3. The snowfall volume is the accumulated snowfall with the rate estimated by Eq.(2) from radar reflectivity at the lowest bin. Over half (67.4%) of the observed samples are near-surface snowfall, followed by shallow (21.2%) and then deep (11.4%) snowing clouds. However, deep snowing clouds contribute the most to the total snowfall volume (45.3%), followed by shallow (28.5%) and then near-surface (26.2%) snowing clouds. Pettersen et al. (2020) analyzed snowing clouds observed by a micro rain radar at Marquette, Michigan for 4 winter seasons. Snow clouds are divided into shallow (top height lower than 1.5 km) and deep events. They found that shallow clouds occur 2 times as often as deep clouds while both types contribute almost equally to annual snowfall accumulation. Those statistics are very similar to the results obtained in this study for snowfall events observed at Pyeongchang, Korea. Kulie et al. (2016) found that globally shallow snow clouds can be associated with strong convections and heavy snowfall. The snowfall rates for shallow and near-surface snow clouds observed in this study are mostly lower than 0.5 mm h^{-1}; heavy snowfall is mainly associated with deep snow clouds. One possible explanation of the difference is as follows. The snowfall from shallow and near-surface snow clouds in this study mostly comes from convections associated with cold airmass outbreak from the northwest. Since the observation site is in the mountains in the east coastal region of the Korean Peninsula, substantial portion of the moisture picked up by the cold air from the warm ocean in the Yellow Sea (west of the Korean Peninsula) has been already transformed to snow before reaching the observation site. In addition, the convective clouds and easterly flow can cross the mountains and produce heavy snowfall over the site in the case of strong winds and lower thermal stability. However, these types of events occurred relatively infrequently during the experiment when compared to the other snowfall types. Consequently, the snowfall associated with shallow and near-surface clouds at this site is relatively moderate.

3. Microphysical Properties of Snowing Clouds

3.1 Case Examples

(a) Deep and "dry" followed by near-surface snowing clouds

From 7 to 8 March 2018, a low-pressure system passed the south of the Korea Peninsula, and solid precipitation was observed at the radar site from 09 UTC on the 7th through 24 UTC on the 8th. In Fig.4 shown are cross section of radar reflectivity and time variation of liquid water path and snow water path (SWP, vertically integrated snow water content). Surface PARSIVEL and 2DVD observations indicated that snow particle types are mostly snowflakes from 09 UTC on the 7th to 06 UTC on the 8th, while rimed ice particles and graupels are also observed then after. The radar and radiometer observations indicate that the deep clouds have cloud top higher than 8 km and peak snow water path value about 500 g m^{-2}. However, liquid water in the deep clouds is low, with liquid water path constantly below 150 g m^{-2}. Once the deep clouds pass the station, the clouds became much shallower, mostly being classified as near-surface snowing clouds. However, their liquid water path increased substantially with peak values close to 600 g m^{-2}, which is consistent with the observed rimed ice particles and graupels during this period.

(b) Deep and "wet" followed by shallow snowing clouds

On 28 February 2018, deep snowing clouds associated with a low-pressure system were observed at the radar site, followed by shallow snowing clouds that lasted till 03 UTC on March 1. Radar reflectivity, liquid water path and snow water path are shown in Fig.5. Surface PARSIVEL observations indicated melting snow with surface air temperature near 0ºC before 04 UTC on February 28, which may have contributed the liquid water path peak around 04 UTC. Heavy snowfall was observed from 04 to 14 UTC on 28 February; snowflakes observed at surface are large aggregates and show indications of riming occurred. Liquid water path was high for both the deep and shallow clouds with peaks higher than 400 g m^{-2} even without including the portion of melting snow before 04 UTC on the 28th. Rimed snow particles were observed at surface corresponding to the shallow snow cell based on 2DVD and MASC data.

3.2 Liquid versus Ice in Snowing Clouds

During the 6-month period, a total of 374 hours of snow precipitation have been observed by the RPG-FMCW. The frequency distributions of 5-minute averaged surface snowfall rate and liquid water path are shown in Fig.6 with both surface snowfall rate and liquid water path in logarithm scale. On average, deeper clouds generate heavier snowfall; near-surface and shallow snowing clouds produce snowfall rarely heavier than 0.5 mm h^{-1}, while snowfall rate in deep snowing clouds reaches over 1 mm h^{-1}. Higher values of cloud liquid water path are also more likely observed in deeper clouds. However, the likelihood of a substantial amount of liquid water in shallower clouds is also high. For example, for the liquid water path range of 100~250 g m^{-2} the frequency values are still reaching about 10% for near-surface and shallow snowing clouds. On the upper limit, liquid water path in all clouds only occasionally exceeds 500 g m^{-2}.

In Fig.7, we show the scatterplot of surface snowfall rate versus liquid water path averaged over a 5-minute period. As indicated in case studies earlier, the two variables hardly vary in a correlated fashion, neither positively nor negatively. For deep snowing clouds, the heaviest snowfall corresponds to a liquid water path of about 200 g m^{-2}, while further increasing in liquid water path does not seem to enhance surface snowfall. For shallow and near-surface snowing clouds, the snowfall rate is confined between 0 to 0.6 mm h^{-1} while liquid water path stretches from 0 to 600 g m^{-2} without coherent variation between liquid water path and surface snowfall rate. Additionally, unlike heavy snowfall preferably occurring in deep snowing clouds, large values of liquid water path (say > 300 g m^{-2}) are almost equally probable to be found in near-surface, shallow and in deep snowing clouds.

The mean state and its variability of cloud liquid water are also examined in the 2-dimensional space of near surface radar reflectivity and cloud top height, as shown in Fig.8. In this figure, the mean values of (a) the number of occurrences, (b) liquid water path, and (c) standard deviation of liquid water path in each 2 dBZ by 500 m grid are shown based on the 5-minute averaged data. The number of occurrences diagram indicates that heavier snowfall (stronger radar reflectivity) tends to have a higher cloud top for cases with near surface radar reflectivity greater than 0 dBZ although this tendency is not clear for cases with lower values of near surface radar reflectivity. The diagrams for mean and standard deviation of liquid water path shown in Figs.8b and 8c appear to indicate the following. For deep snow clouds (top higher than 4 km) with surface radar reflectivity greater than 6 dBZ, liquid water path has a large mean value but a small standard deviation. On the other hand, shallow snow clouds (top between 1.5 and 4 km) with moderate surface radar reflectivity (0-5 dBZ) have a moderate mean value but a high variability of liquid water path. There is an area with high mean value and high variability of liquid water path located at surface radar reflectivity between -10 and 0 dBZ and cloud top height between 4 and 6 km, possibly corresponding to convective cells in early developing stage. For near-surface and shallow clouds, both the mean value and standard deviation of liquid water path appear to increase as surface radar reflectivity increases.

To express the "dryness" of the snowing clouds, one may use the glaciation ratio (GR) defined as (Liu and Takeda, 1988):

$$GR = \frac{SWP}{LWP+SWP} \times 100\% \,. \qquad (5)$$

The GR parameter indicates the fraction of total condensed water in the column that has been converted to solid phase. In Fig.9, we show how the GR values are related to (a) cloud top height, (b) surface snowfall rate and (c) cloud mean temperature (temperature at the geometrical middle of a reflectivity profile). Generally speaking, clouds with higher tops, associated with higher snowfall rate or with colder mean temperature tend to have higher degrees of glaciation, although the scatters are extremely large. For example, for a shallow snowing cloud with 0.2 mm h^{-1} snowfall rate, its glaciation ratio can be any value from near 0 to about 100%, probably depending on the development stage of individual cells. In Fig.9a, there is a concentration of points with high cloud top (>5 km) but glaciation ratio between 50% and 75% rather than 100%. It is likely that the phenomena are caused by clouds that have multiple layers or a cloud layer with dynamically decoupled upper and lower portions. Corresponding to the clouds with their heaviest snowfall rate, deep snowing clouds have a glaciation ratio of about 60% while shallow and near-surface snowing clouds only have their glaciation ratio less than 20%, which adds extra difficulties for detecting snow in these types of clouds by passive microwave observations. There is loosely a trend that clouds with a lower mean temperature have a higher degree of glaciation. For near-surface snowing clouds, this trend is less clear with their glaciation degree hardly over 50%. Using data observed over Greenland, Pettersen et al. (2018) found that snowfall events for frontal deep clouds are often ice clouds with little liquid water while shallower clouds are typically mixed-phase clouds and contain plenty of supercooled liquid water. Their low glaciation rate for shallower clouds is similar to the result of this study.

3.3 Vertical Structures

The mean vertical structure of the snowing clouds may be expressed by contoured frequency by altitude diagrams (CFADs; Yuter and Houze, 1995) of radar reflectivity, mean Doppler velocity, and Doppler spectral width, as shown in Fig. 10. For deep snowing clouds, the radar reflectivity CFADs show a relatively narrow spread with a sharp radar reflectivity decreases with the increase of altitude above 4 km ("left-tilting" structure), implying that most of the precipitation growth occurs above 4 km. For shallow clouds, the "left-tilting" structure starts from near surface and the frequency has broader distribution at each level. In contrast, the near-surface snowing clouds do not show such "left-tilting" structure, but rather have a broad distribution below their cloud top height, indicating that the precipitation maximum does not necessarily situate near the surface in these profiles. We interpret that the broad distribution of frequencies at each level is likely due to the convective nature of these clouds, so that the precipitation profile is largely determined by the development stage of the clouds. For example, developing clouds have their precipitation maximum in the upper portion while matured clouds have their precipitation maximum in the lower portion in the vertical profiles.

For mean Doppler velocity, the most likely values are around -1 m s^{-1} (the negative sign indicates downward movement), corresponding to the terminal velocity of unrimed to moderately rimed aggregates (Locatelli and Hobbs, 1974). There is a tendency that particles in upper levels fall somewhat slower than those in the lower levels. The Doppler spectral width indicates that particles in the upper levels have a narrower spectrum. Combining the vertical profiles of mean Doppler velocity and spectral width, it is concluded that ice particles at upper levels have a narrower size distribution and lower terminal velocity. It is also interesting to notice that there seems to be a regime shift for deep snow clouds near 4 km altitude; the frequency patterns appear to be different below and above this level for all the CFADs of radar reflectivity, Doppler velocity and spectrum width. Additionally, the slope of reflectivity suddenly changes around 8 km and the absolute value of Doppler velocity reduced dramatically below 8 km. A similar feature also appeared in the long-term observation with cloud radar (see Figs. 16 and 17 of Ye et al. 2020). The shift of growth regime was appeared at 8 km height (3~3.5 km above the bright band peak and corresponding to ~ -17°C). This regime shift induced the updraft (reached 1 m s^{-1}) below this layer. However, Ye et al. (2020) could not explain the linkage between this regime shift and updraft below. While it is beyond the scope of this study, this phenomenon will be an interesting topic for future research on the cloud microphysics in this region.

4. Implications to Passive Microwave Remote Sensing

To understand how the microphysical properties in snowing clouds impact on passive microwave remote sensing, a radiative transfer model simulation at GPM/GMI channels has been conducted using the measured liquid and snow water quantities as a guidance for the model input. The radiative transfer model developed by Liu (1998) has been used in this simulation, which uses a four-stream discrete ordinates method to solve the radiative transfer equation. For snow particles, the single-scattering properties calculated by discrete dipole approximation for sector type snowflakes (Liu, 2008b) are used. Based on studies of Geer and Baordo (2014), the single-scattering properties for the sector type snowflakes work reasonably well in radiative transfer simulations for middle latitude snowstorms. Since the emphasis of this study is to assess the impact of cloud microphysics on satellite remote sensing, the variability of surface emissivity is not considered. In all the following simulations, we assign an emissivity of 0.9 for land surface for all GMI channels and a 5 m s^{-1} wind speed over ocean to compute surface emissivity.

4.1 Masking Effect to Scattering Signatures by Cloud Liquid Water

Based on analysis shown in section 3.2, liquid water path frequently varies from 0 to 500 g m^{-2} for any of the 3 types of snowing clouds while snowfall rate at surface commonly reaches to 0.3, 0.5, and 1.0 mm h^{-1}, respectively, for near-surface, shallow, and deep clouds. We examine how the cloud liquid would mask the ice scattering at two GMI frequencies, 89 and 166 GHz, at viewing angles of 53° for 89 GHz and 49° for 166 GHz using radiative transfer calculations. Using clear-sky brightness temperature T_{B0} as the base, Figure 11 shows how brightness temperature varies as liquid water path and surface snowfall rate increase. Note that in these radiative transfer calculations, mean snowfall rate profiles derived from observations are used. The mean profiles are derived as follows. We first group all the observed snowfall rate profiles according to their cloud type, and then for each cloud type we average those profiles that fall into a given snowfall rate bin. A 1-km deep liquid cloud layer is placed at 0.5-1.5 km, 2.5-3.5 km and 4.5-5.5 km, respectively, for near-surface, shallow, and deep clouds. The liquid water path is increased from 0 to 500 g m^{-2}.

For near-surface snowing clouds, the decrease of brightness temperature due to ice scattering is very limited for either 89 or 166 GHz, only about 1.5 K for 89 GHz and 2.5 K for 166 GHz occurring when liquid water path is very low. Therefore, most likely this type of clouds displays a warming signature in the passive microwave observations due to the existence of liquid water clouds. For shallow snowing clouds, the modeling results show there is still a mostly warming at 89 GHz and an equal mix of warming and cooling at 166 GHz. The masking effect still remains quite significant at 89 GHz even for deep snowing clouds; it can cause an increase in brightness temperature by more than 5 K from clear-sky value. The dominant scattering signature shows at 166 GHz for deep clouds. At surface snowfall rate of 1 mm h^{-1}, brightness temperature can decrease from clear-sky value by more than 30 K (color bar only shows up to -15 K) when liquid water path is lower than 100 g m^{-2}.

Based on the above modeling results, it is clear that if only relying on scattering signature, i.e., brightness temperature depression, an algorithm will totally fail in retrieving snowfall rate for near-surface clouds and partially fail for shallow clouds. Even for deep snowing clouds, cloud liquid water will impact snowfall retrieval with a result of an overestimation for low and an underestimation for high values of liquid water path. Therefore, a more plausible approach to the retrieval problem is to use a statistical method in which the algorithm utilizes any regularities naturally existing between cloud liquid and snow profiles to search for the most likely snowfall rate. One such approach is the Bayesian retrieval algorithm (Kummerow et al., 1996; Olson et al., 1996; Seo and Liu, 2005). This approach requires that the *a priori* database used in the retrieval has the same characteristics in both microphysical properties and occurring frequency as those in natural clouds.

4.2 A Bayesian Retrieval Exercise

In this section, an idealized experiment is designed to examine how a Bayesian retrieval algorithm would perform for the three types of snowing clouds if we only take into account the error caused by the variability of liquid water path and snowfall rate profiles. In other words, we examine how well a Bayesian retrieval algorithm would perform, when assuming no variations in surface emissivity, snowflakes being a fixed type, and particle size distribution following an exponential form. Therefore, this exercise mainly assesses the problems caused by the uncertainties associated with cloud liquid and snow amounts.

First, a total of 30870 5-minute averaged snow profiles are constructed from the 6 months long surface radar observations (including zero snowfall profiles). Each of the snow profile is accompanied with a liquid water path which is assigned to be a 1 km deep layer at 0.5-1.5 km, 2.5-3.5 km and 4.5-5.5 km, respectively, for near-surface, shallow, and deep clouds. Atmospheric temperature, pressure, and relative humidity profiles are also assigned to these profiles by interpolating MERRA-2 data spatially and temporally to the individual snow profiles. A radiative transfer model calculation is then performed to generate brightness temperatures at 11 GMI channels (all except the 10.7 GHz GMI channels) using the above profiles as input. The 10.7 GHz channel is not considered here because its brightness temperature is not sensitive to either liquid or ice hydrometeors and its GMI channel has too large a footprint size compared to other channels. It is also assumed that surface skin temperature is the same as surface air temperature and surface emissivity is a constant (0.9 for land) for all channels. A sector type snowflake (Liu, 2008b) and an exponential particle size distribution (Sekhon and Srivastava, 1971) are used for all the cases. We then randomly divided the 30870 profiles and their computed brightness temperatures into two equal-number groups; one is used as the *a priori* database for the Bayesian retrieval algorithm, and the other as "observations" to test how well the surface snowfall rate can be retrieved from the "measured" brightness temperatures. To mimic a possible random error in the measured brightness temperatures, a random noise with a maximum magnitude of 1 K is added to the "measured" brightness temperatures before retrieval is performed. A detailed description of the Bayesian retrieval method can be found in Seo and Liu (2005).

In Fig.12 shown are the scatterplots of "measured" versus retrieved surface snowfall rate, separated by snow cloud types. The correction as indicated by R^2 (square of linear correlation coefficient), bias and root-mean-square (rms) difference are shown in each diagram. The biases between the "measured" and retrieved snowfall rate are small for all snow cloud types, with values of 0.019, 0.033, and 0.03 mm h^{-1} for near-surface, shallow and deep snowing clouds, respectively. The values of rms differences are also small; they are 0.05, 0.11, and 0.16 mm h^{-1}, respectively, for near-surface, shallow and deep snowing clouds. The color of the points in the figures indicates the value of liquid water path associated with individual profiles. Clearly, as the cloud layer deepens, the skill of the retrieval improves. The values of R^2 increases from 0.32 for near-surface clouds, to 0.41 for shallow clouds, and to 0.62 for deep clouds. That is, the retrievals can resolve 32%, 41%, and 62% of the variances in snowfall rate observations for near-surface, shallow and deep clouds, respectively.

A question one may naturally want to ask is: Will the retrieval skill be improved if the same clouds were moved to areas over ocean where liquid water information is distinguishable at some microwave channels (e.g., 89 GHz)? To answer this question, we perform the same retrieval exercise as mentioned above but assuming the clouds are over an ocean surface with a constant surface wind speed of 5 m s^{-1}. Similarly, half of the 30870 samples are used as a priori database and half as "observations". The retrieval results are shown in Fig.13. Similar to land cases, the biases and rms differences have small values for all cloud types. For deep snowing clouds, the R^2 statistic indicates only small improvement in retrieval skills between over land and over ocean cases, although a visual inspection of the scatterplot shows that a better correspondence between "measured" and retrieved values at snowfall rates lower than 0.2 mm h^{-1}. The improvement in retrieval skills for over ocean shallow clouds is moderate with R^2 of 0.54 versus 0.41 over land. The most significant improvement in retrieval skills occurs for over ocean near-surface snowing clouds, in which R^2 increases from 0.32 over land to 0.52 over ocean. Note that land surface emissivity and ocean surface wind are fixed in the retrieval exercises. Therefore, the improvement is not due to a better knowledge of surface conditions, but rather due to the richer information content on cloud microphysics contained in "measured" brightness temperatures over ocean. One such piece of information must have come from the brightness temperature difference between two polarizations over ocean, which remines mostly zero over land surfaces. The results shown in Fig.13 indicate that the extra polarization information helps the most for retrieving snowfall in shallower clouds.

In Figs. 12 and 13, it is also noted that an underestimation occurs when snowfall rate is greater than 0.7 mm h^{-1} for deep snowing clouds regardless over land or ocean. This underestimation may be due to the deficiency of the Bayesian scheme, in which the retrieval is a weighted average of snowfall rates of datum points in the *a priori* database that are radiometrically consistent with observations. When an observation is close to the upper boundary (i.e., high snowfall rates) in the database, the averaging takes a greater number of datum points with snowfall rates lower than the actual value than those with higher snowfall rates (no more datum points beyond upper boundary), thus resulting in an underestimation.

To understand the information conveyed in polarization difference of brightness temperatures, we performed a similar simulation to that described in Section 4.1, but replaced land surface to ocean surface with a wind speed of 5 m s^{-1}. The changes of depolarization as liquid water path and snowfall rate increase are shown in Fig.14 for each of the 3 cloud types at 89 and 166 GHz. Depolarization is defined as $\Delta T_B = T_{BV} - T_{BH}$, where T_{BV} and T_{BH} are brightness temperatures at vertical and horizontal polarizations, respectively. The change is relative to clear-sky values, ΔT_{B0}. The change in depolarization at 89 GHz is well corresponding to the change in liquid water path, without much dependence on snowfall rate, particularly for near-surface and shallow snowing clouds.

Therefore, it is plausible that the increased retrieval skill over ocean for near-surface and shallow clouds is due to the added information on liquid water contained in the polarization differences. Comparing Figs.12 and 13, it seems that the added information is particularly helpful in improving retrievals at low snowfall rates.

5. Conclusions

During the 2017-18 winter season, a ground-based radar and radiometer observation has been carried out over Korean Peninsula as part of the ICE-POP 2018 campaign. Using the coincident radar and radiometer data, we were able to retrieve cloud liquid water path, snow water content and snowfall rate. These microphysical properties and their relation to cloud top height are analyzed in an effort to better understand their implications to satellite remote sensing of snowfall. In the analysis, we divide the approximately 374 hours of observed snowing clouds into near-surface, shallow and deep types, for which the cloud top height is below 1.5 km, between 1.5 and 4 km and above 4 km, respectively. The near-surface snowing clouds are most likely to be missed by currently available space-borne radars because of the blind zone caused by the contamination of surface clutter, and their shallowness and liquid water abundance may also present challenges to satellite radiometer observations. In this region during the observation period, the shallow snowing clouds commonly occur in unstable air mass after the passing of a cold front. It can be detected by space-borne radars with sufficient low minimum detectable radar reflectivity, but the mixture of cloud liquid emission and ice scattering complicates the retrievals by passive microwave observations. The deep snowing clouds are mostly located near frontal zones and low-pressure centers; their strong ice scattering signature makes it the most favorable type among the three for snowfall retrievals by both satellite radars and radiometers. Surveying all the observed data, it is found that near-surface snowing cloud is the most frequently observed cloud type with a frequency of occurrence over 60%, while deep snowing cloud contributes the most in snowfall volume with about 50% of the total snowfall amount.

The probability distributions of surface snowfall rates are clearly different among the three types of snowing clouds, with vast majority of them hardly reaching to 0.3 mm h^{-1} for near-surface, 0.5 mm h^{-1} for shallow, and 1 mm h^{-1} for deep snowing clouds. However, liquid water path in the three types of snowing clouds all has substantial likelihood to be between 0 to 500 g m^{-2}, although deeper clouds are somewhat more likely with more liquid water as well. There is no clear correlation, either positive or negative, between surface snowfall rate and liquid water path. However, given the same surface snowfall rate, clouds with lower cloud top height tend to have higher liquid water path. The glaciation ratio defined by the ice fraction in the total condensed water in an atmospheric column is estimated and found to be related to cloud top height, surface snowfall rate and cloud mean temperature, although the relations are very scattered. A higher value of glaciation ratio is generally corresponding to a higher cloud top, a higher surface snowfall rate and lower cloud mean temperature.

Moreover, we examined the ability of a Bayesian type algorithm to retrieve surface snowfall rate for snow events similar to those observed in this study when using GPM/GMI observations. First, using the approximately 30,000 observed snow cloud and precipitation-free profiles, brightness temperatures at GPM/GMI channels are computed. Then, these snowfall rate and associated brightness temperature pairs are randomly divided into two groups. One group is used as "observations" and the other is used as the *a priori* database of the Bayesian algorithm. Under idealized scenario, i.e., without considering the uncertainties caused by surface emissivity, ice particle size distribution and particle shape, the examination results indicate that the correlation as expressed by R^2 between the "retrieved" versus "measured" snowfall rates is about 0.32, 0.41 and 0.62, respectively, for near-surface, shallow and deep snowing clouds over land surface. Since this is an extremely idealized retrieval exercise only dealing with the complicated mixture of cloud liquid and snow profiles, these numbers basically indicate the upper limits of how a retrieval algorithm can perform for these snowing clouds. A hypothetical retrieval for the same clouds but over ocean is also studied, and a major improvement in skill for near-surface clouds is found with R^2 increased from 0.32 to 0.52, while improvement in skill is small for deeper clouds. The improvement is interpreted as that some liquid water information is resolved by the polarization difference contained in the over-ocean brightness temperatures.

This information helps the most for the otherwise information-poor observations for the near-surface clouds.

By analyzing the radar and radiometer data from one-winter-long observations and the results of a Bayesian retrieval dry run, this study gives a general picture of the characteristics of the different types of snowing clouds and points out the fundamental challenges in retrieving their snowfall rate from passive microwave observations. It is hopeful that these results can help developers improve physical assumptions in future algorithms as well as data users better interpret satellite retrieved snowfall products. Lastly, it is worth mentioning that there are still many valuable datasets, such as particle shape and size distribution information from PARSIVEL, 2DVD and MASC, which we didn't analyzed quantitatively in this study. A thorough analysis of those datasets in conjunction with the remote sensing data will undoubtably improve future snowfall retrieval algorithm development.

Data availability. Surface radar and radiometer data were obtained during ICE-POP 2018 by the authors.

Author contributions. Data collection are made by Lee, Kim, Seo and Jeoung. Radiative transfer modeling and manuscript writing are primarily done by Liu and Jeoung. Interpretation of results are shared by all authors.

Competing interests. The authors declare that they have no conflict of interest.

Acknowledgements. This research has been supported by NASA under grants 80NSSC19K0718 and NNX16AP27G. Participation of KK and GWL has been supported by the Korea Meteorological Administration Research and Development Program under Grant KMI2020-00910, and by the Korea Environmental Industry & Technology Institute (KEITI) of the Korea Ministry of Environment (MOE) as "Advanced Water Management

Research Program" (79615). The authors are greatly appreciative to the participants of the World Weather Research Programme Research Development Project and Forecast Demonstration Project, International Collaborative Experiments for Pyeongchang 2018 Olympic and Paralympic winter games (ICE-POP 2018), hosted by the Korea Meteorological Administration.

References

Battaglia, A., Rustemeier, E., Tokay, A., Blahak, U. and Simmer, C.: PARSIVEL snow observations: A critical assessment, J. Atmos. Ocean. Technol., doi:10.1175/2009JTECHA1332.1, 2010.

Bennartz, R. and Bauer, P.: Sensitivity of microwave radiances at 85-183 GHz to precipitating ice particles, Radio Sci., 38(4), n/a-n/a, doi:10.1029/2002rs002626, 2003.

Casella, D., Panegrossi, G., Sanò, P., Marra, A. C., Dietrich, S., Johnson, B. T. and Kulie, M. S.: Evaluation of the GPM-DPR snowfall detection capability: Comparison with CloudSat-CPR, Atmos. Res., 197, 64–75, doi:10.1016/j.atmosres.2017.06.018, 2017.

Chen, H., Chandrasekar, V. and Bechini, R.: An improved dual-polarization radar rainfall algorithm (DROPS2.0): Application in NASA IFloodS field campaign, J. Hydrometeorol., doi:10.1175/JHM-D-16-0124.1, 2017.

Chen, S., Hong, Y., Kulie, M., Behrangi, A., Stepanian, P. M., Cao, Q., You, Y., Zhang, J., Hu, J. and Zhang, X.: Comparison of snowfall estimates from the NASA CloudSat Cloud Profiling Radar and NOAA/NSSL Multi-Radar Multi-Sensor System, J. Hydrol., 541, 862–872, doi:10.1016/j.jhydrol.2016.07.047, 2016.

Chung, S.-H., Byun, K.-Y., Lee, T.-Y.: Classification of snowfalls over the Korean peninsula based on developing mechanism. Atmosphere. 16, 33–48, 2006.

Draine, B. T. and Flatau, P. J.: Discrete-Dipole Approximation For Scattering Calculations, J. Opt. Soc. Am. A, 11(4), 1491, doi:10.1364/josaa.11.001491, 1994.

Garrett, T. J., Fallgatter, C., Shkurko, K. and Howlett, D.: Fall speed measurement and high-resolution multi-angle photography of hydrometeors in free fall, Atmos. Meas.

Tech., doi:10.5194/amt-5-2625-2012, 2012.

Geer, A. J. and Baordo, F.: Improved scattering radiative transfer for frozen hydrometeors at microwave frequencies, Atmos. Meas. Tech., doi:10.5194/amt-7-1839-2014, 2014.

Gehring, J., Oertel, A., Vignon, É., Jullien, N., Besic, N., and Berne, A.: Microphysics and dynamics of snowfall associated with a warm conveyor belt over Korea, Atmos. Chem. Phys., 20, 7373–7392, https://doi.org/10.5194/acp-20-7373-2020, 2020.

Gelaro, R., McCarty, W., Suárez, M. J., Todling, R., Molod, A., Takacs, L., Randles, C. A., Darmenov, A., Bosilovich, M. G., Reichle, R., Wargan, K., Coy, L., Cullather, R., Draper, C., Akella, S., Buchard, V., Conaty, A., da Silva, A. M., Gu, W., Kim, G. K., Koster, R., Lucchesi, R., Merkova, D., Nielsen, J. E., Partyka, G., Pawson, S., Putman, W., Rienecker, M., Schubert, S. D., Sienkiewicz, M. and Zhao, B.: The modern-era retrospective analysis for research and applications, version 2 (MERRA-2), J. Clim., 30(14), 5419–5454, doi:10.1175/JCLI-D-16-0758.1, 2017.

Gong, J. and Wu, D. L.: Microphysical properties of frozen particles inferred from Global Precipitation Measurement (GPM) Microwave Imager (GMI) polarimetric measurements, Atmos. Chem. Phys., 17(4), 2741–2757, doi:10.5194/acp-17-2741-2017, 2017.

Grazioli, J., Genthon, C., Boudevillain, B., Duran-Alarcon, C., Del Guasta, M., Madeleine, J. B. and Berne, A.: Measurements of precipitation in Dumont d'Urville, Adélie Land, East Antarctica, Cryosphere, doi:10.5194/tc-11-1797-2017, 2017.

Honeyager, R., Liu, G. and Nowell, H.: Voronoi diagram-based spheroid model for microwave scattering of complex snow aggregates, J. Quant. Spectrosc. Radiat. Transf., 170, 28–44, doi:10.1016/j.jqsrt.2015.10.025, 2016.

Hudak, D., Rodriguez, P. and Donaldson, N.: Validation of the CloudSat precipitation occurrence algorithm using the Canadian C band radar network, J. Geophys. Res., 113, D00A07, doi:10.1029/2008JD009992, 2008.

Katsumata, M., Uyeda, H., Iwanami, K. and Liu, G.: The response of 36- and 89-GHz microwave channels to convective snow clouds over ocean: Observation and modeling, J.

Appl. Meteorol., 39(12 PART 2), 2322–2335, doi:10.1175/1520-0450(2000)039<2322:troagm>2.0.co;2, 2000.

Kim, M. J., Weinman, J. A., Olson, W. S., Chang, D. E., Skofronick-Jackson, G. and Wang, J. R.: A physical model to estimate snowfall over land using AMSU-B observations, J. Geophys. Res. Atmos., doi:10.1029/2007JD008589, 2008.

Kim, J., Yoon, D., Cha, D. H., Choi, Y., Kim, J. and Son, S. W.: Impacts of the East Asian winter monsoon and local sea surface temperature on heavy snowfall over the Yeongdong region, J. Clim., 32(20), 6783–6802, doi:10.1175/JCLI-D-18-0411.1. 2019.

Kim, T., and Jin, E. K.: Impact of an interactive ocean on numerical weather prediction: A case of a local heavy snowfall event in eastern Korea, J. Geophys. Res. Atmos., 121, 8243–8253, doi:10.1002/2016JD02476, 2016.

Ko, A.-R., Kim, B.-G., Eun, S.-H., Park, Y.-S. and Choi, B.-C.: Analysis of the relationship of water vapor with precipitation for the winter ESSAY (Experiment on Snow Storms At Yeongdong) period, Atmosphere, 26(1), 19–33, doi:10.14191/atmos.2016.26.1.019, 2016.

Kongoli, C., Meng, H., Dong, J. and Ferraro, R.: A snowfall detection algorithm over land utilizing high-frequency passive microwave measurements—Application to ATMS, J. Geophys. Res., doi:10.1002/2014JD022427, 2015.

Kneifel, S., Löhnert, U., Battaglia, A., Crewell, S. and Siebler, D.: Snow scattering signals in ground-based passive microwave measurements. J. Geophys. Res., 115, D16214. doi:10.1029/2010JD013856, 2010.

Kneifel, S, Redl, S., Orlandi, E., Löhnert, U., Cadeddu, M. P., Turner, D. D., and Chen, M.-T.: Absorption Properties of Supercooled Liquid Water between 31 and 225 GHz: Evaluation of Absorption Models Using Ground-based Observations, J. Appl. Meteor. Climatol., 53, 1028-1045. doi:10.1175/JAMC-D-13-0214.1, 2014.

Kruger, A. and Krajewski, W. F.: Two-dimensional video disdrometer: A description, J. Atmos. Ocean. Technol., doi:10.1175/1520-0426(2002)019<0602:TDVDAD>2.0.CO;2, 2002.

Küchler, N., Kneifel, S., Löhnert, U., Kollias, P., Czekala, H. and Rose, T.: A W-band radar–radiometer system for accurate and continuous monitoring of clouds and precipitation. J. Atmos. Oceanic Technol., 34, 2375–2392. doi: 10.1175/JTECHD-17-0019.1, 2017.

Kulie, M. S. and Bennartz, R.: Utilizing spaceborne radars to retrieve dry Snowfall, J. Appl. Meteorol. Climatol., 48(12), 2564–2580, doi:10.1175/2009JAMC2193.1, 2009.

Kulie, M. S., Milani, L., Wood, N. B., Tushaus, S. A., Bennartz, R., L'Ecuyer, T. S. and L'Ecuyer, T. S.: A shallow cumuliform snowfall census using spaceborne radar, J. Hydrometeorol., 17(4), 1261–1279, doi:10.1175/JHM-D-15-0123.1, 2016.

Kummerow, C., Oison, W. S. and Giglio, L.: A simplified scheme for obtaining precipitation and vertical hydrometeor profiles from passive microwave sensors, IEEE Trans. Geosci. Remote Sens., doi:10.1109/36.536538, 1996.

Kummerow, C. D., Randel, D. L., Kulie, M., Wang, N. Y., Ferraro, R., Joseph Munchak, S. and Petkovic, V.: The evolution of the goddard profiling algorithm to a fully parametric scheme, J. Atmos. Ocean. Technol., doi:10.1175/JTECH-D-15-0039.1, 2015.

Liebe, H. J., Hufford, G. A.,, and Cotton, M. G.: Propagation modeling of moist air and suspended water/ice particles at frequencies below 1000 GHz, AGARD Conf. Proc.,542,3-1–3-10,1993.

Liu, G.: A fast and accurate model for microwave radiance calculations, J. Meteorol. Soc. Japan, doi:10.2151/jmsj1965.76.2_335, 1998.

Liu, G.: Approximation of Single Scattering Properties of Ice and Snow Particles for High Microwave Frequencies, J. Atmos. Sci., 61(20), 2441–2456, doi:10.1175/1520-0469(2004)061<2441:AOSSPO>2.0.CO;2, 2004.

Liu, G.: Deriving snow cloud characteristics from CloudSat observations, J. Geophys. Res. Atmos., 114(8), 1–13, doi:10.1029/2007JD009766, 2008a.

Liu, G.: A database of microwave single-scattering properties for nonspherical ice particles, Bull. Am. Meteorol. Soc., 89(10), 1563–1570, doi:10.1175/2008BAMS2486.1, 2008b.

Liu, G. and Curry, J. A.: Precipitation characteristics in Greenland-Iceland-Norwegian Seas determined by using satellite microwave data and modeling studies that require Observations Salinity satellite retrievals are the only platform from described by Schmitt cycle for tropical , , 102, 987–997, 1997.

Liu, G. and Seo, E.-K. K.: Detecting snowfall over land by satellite high-frequency microwave observations: The lack of scattering signature and a statistical approach, J. Geophys. Res. Atmos., 118(3), 1376–1387, doi:10.1002/jgrd.50172, 2013.

Liu, G. and Takeda, T.: Interesting findings on the precipitation of middle-level stratiform clouds in recent years are a banded mesoscale structure of rainfall and a showed that precipitation is initiated in high-level clouds (" seeder " clouds) and it is enhanced in deep stra, , (October), 645–660, 1988.

Locatelli, J. D. and Hobbs, P. V.: Fall speeds and masses of solid precipitation particles, J. Geophys. Res., doi:10.1029/jc079i015p02185, 1974.

Löffler-Mang, M. and Joss, J.: An optical disdrometer for measuring size and velocity of hydrometeors, J. Atmos. Ocean. Technol., doi:10.1175/1520-0426(2000)017<0130:AODFMS>2.0.CO;2, 2000.

Marchand, R., Mace, G. G., Ackerman, T. and Stephens, G.: Hydrometeor detection using Cloudsat - An earth-orbiting 94-GHz cloud radar, J. Atmos. Ocean. Technol., 25(4), 519–533, doi:10.1175/2007JTECHA1006.1, 2008.

Meng, H., Dong, J., Ferraro, R., Yan, B., Zhao, L., Kongoli, C., Wang, N. Y. and Zavodsky, B.: A 1DVAR-based snowfall rate retrieval algorithm for passive microwave radiometers, J. Geophys. Res., 122(12), 6520–6540, doi:10.1002/2016JD026325, 2017.

Nam, H. G., Kim, B. G., Han, S. O., Lee, C. and Lee, S. S.: Characteristics of easterly-induced snowfall in Yeongdong and its relationship to air-sea temperature difference, Asia-Pacific J. Atmos. Sci., 50(4), 541–552, doi:10.1007/s13143-014-0044-3, 2014.

Noh, Y. J., Liu, G., Seo, E. K., Wang, J. R. and Aonashi, K.: Development of a snowfall retrieval algorithm at high microwave frequencies, J. Geophys. Res. Atmos., doi:10.1029/2005JD006826, 2006.

Olson, W. S., Kummerow, C. D., Heymsfield, G. M. and Giglio, L.: A method for combined passive-active microwave retrievals of cloud and precipitation profiles, J. Appl. Meteorol., 35(10), 1763–1789, doi:10.1175/1520-0450(1996)035<1763:AMFCPM>2.0.CO;2, 1996.

Park, H., Lee, J., Chang, E.: High-resolution simulation of snowfall over the Korean eastern coastal pegion using WRF model: Sensitivity to domain nesting-down strategy. Asia-Pacific J. Atmos. Sci. 55, 493–506. https://doi.org/10.1007/s13143-019-00108-x, 2019.

Pettersen, C., Kulie, M. S., Bliven, L. F., Merrelli, A. J., Petersen, W. A., Wagner, T. J., Wolff, D. B., and Wood, N. B: A composite analysis of snowfall modes from four winter seasons in Marquette, Michigan. J. Appl. Meteor. Climatol., 59(1), 103-124, 2020, doi:/10.1175/JAMC-D-19-0099.1, 2020.

Pettersen, C., Bennartz, R., Merrelli, A. J., Shupe, M. D., Turner, D. D., and Walden, V. P.: Precipitation regimes over central Greenland inferred from 5 years of ICECAPS observations. Atmos. Chem. Phys., 18, 4715-4735. doi:/10.5194/acp-18-4715-2018, 2018.

Rosenkranz, P. W.: Water vapor microwave continuum absorption: A comparison of measurements and models. Radio Sci., 33, 919-928, 1998.

RPG-FMCW: RPG-FMCW-94-SP/DP 94 GHz W-band Cloud Doppler Radar Instrument Installation, Operation and Software Guide (Version 2.10-1). [online] Available from: https://www.radiometer-physics.de/downloadftp/pub/PDF/Cloud Radar/RPG-FMCW-Instrument_Manual.pdf (Accessed 22 January 2020), 2015.

Praz, C., Roulet, Y. A. and Berne, A.: Solid hydrometeor classification and riming degree estimation from pictures collected with a Multi-Angle Snowflake Camera, Atmos. Meas. Tech., doi:10.5194/amt-10-1335-2017, 2017.

Schwartz, M. J.: Observation and Modeling of Atmospheric Oxygen Millimeter-Wave Transmittance, Ph.D. Thesis, Massachusetts Institute of Technology, Department of Physics, 1998.

Sekhon, R. S. and Srivastava, R. C.: Doppler radar observations of drop- size distributions in a thunderstorm, J. Atmos. Sci., 28(6), 983–994, 1971.

Seo, E. K. and Liu, G.: Retrievals of cloud ice water path by combining ground cloud radar and satellite high-frequency microwave measurements near the ARM SGP site, J. Geophys. Res. D Atmos., 110(14), 1–15, doi:10.1029/2004JD005727, 2005.

Sims, E. M. and Liu, G.: A parameterization of the probability of snow-rain transition, J. Hydrometeorol., 16(4), 1466–1477, doi:10.1175/JHM-D-14-0211.1, 2015.

Skofronick-Jackson, G. and Johnson, B. T.: Surface and atmospheric contributions to passive microwave brightness temperatures for falling snow events, J. Geophys. Res. Atmos., 116(2), 1–16, doi:10.1029/2010JD014438, 2011.

Skofronick-Jackson, G., Petersen, W. A., Berg, W., Kidd, C., Stocker, E. F., Kirschbaum, D. B., Kakar, R., Braun, S. A., Huffman, G. J., Iguchi, T., Kirstetter, P. E., Kummerow, C., Meneghini, R., Oki, R., Olson, W. S., Takayabu, Y. N., Furukawa, K. and Wilheit, T.: The Global Precipitation Measurement (GPM) Mission for Science and Society, Bull. Am. Meteorol. Soc., 98(8), 1679–1695, doi:10.1175/BAMS-D-15-00306.1, 2017.

Skofronick-Jackson, G. M., Weinman, J. A., Kim, M. J. and Chang, D. E.: A physical model to determine snowfall over land by microwave radiometry, IEEE Trans. Geosci. Remote Sens., 42(5), 1047–1058, doi:10.1109/TGRS.2004.825585, 2004.

Stephens, G. L., Austin, R. T., Benedetti, A., Mitrescu, C., Vane, D. G., Boain, R. J., Durden, S. L., Mace, G. G. J., Sassen, K., Wang, Z., Illingworth, A. J., O'Connor, E. J., Rossow, W. B. and Miller, S. D.: The cloudsat mission and the A-Train: A new dimension of space-based observations of clouds and precipitation, Bull. Am. Meteorol. Soc., 83(12), 1771-1790+1742, doi:10.1175/BAMS-83-12-1771, 2002.

Tanelli, S., Durden, S. L., Im, E., Pak, K. S., Reinke, D. G., Partain, P., Haynes, J. M. and Marchand, R. T.: CloudSat's cloud profiling radar after two years in orbit: Performance, calibration, and processing, IEEE Trans. Geosci. Remote Sens., 46(11), 3560–3573, doi:10.1109/TGRS.2008.2002030, 2008.

Tang, G., Wen, Y., Gao, J., Long, D., Ma, Y., Wan, W. and Hong, Y.: Similarities and differences between three coexisting spaceborne radars in global rainfall and snowfall estimation, Water Resour. Res., 53(5), 3835–3853, doi:10.1002/2016WR019961, 2017.

Tokay, A., Wolff, D. B. and Petersen, W. A.: Evaluation of the new version of the laser-optical disdrometer, OTT parsivel, J. Atmos. Ocean. Technol., doi:10.1175/JTECH-D-13-00174.1, 2014.

Wang, Y., Chen, Y., Fu, F., and Liu, G.: Identifiction of precipitation onset based on CloudSat observations. J. Quant. Spect. Radiat. Trans., 188, 142-177. doi:10.1016/j.jqsrt.2016.06.028, 2017.

Wang, Y., Liu, G., Seo, E. K. and Fu, Y.: Liquid water in snowing clouds: Implications for satellite remote sensing of snowfall, Atmos. Res., 131, 60–72, doi:10.1016/j.atmosres.2012.06.008, 2013.

Wood, N. B., L'Ecuyer, T. S., Vane, D. G., Stephens, G. L. and Partain, P.: Level 2C snow profile process description and interface control document, version 0, CloudSat Proj., (D), 21 [online] Available from: http://www.cloudsat.cira.colostate.edu/ICD/2C-SNOW-PROFILE/2C-SNOW-PROFILE_PDICD_P_R04.pdf, 2013.

Ye, B.-Y., Jung, E., Shin, S., and Lee, G.: Statistical Characteristics of Cloud Occurrence and Vertical Structure Observed by a Ground-Based Ka-Band Cloud Radar in South Korea. *Remote Sens., 12*, 2242, doi:10.3390/rs12142242, 2020.

Yin, M. and Liu, G.: Developing an a priori database for passive microwave snow water retrievals over ocean, J. Geophys. Res. Atmos., 122(23), 12,960-12,981, doi:10.1002/2017JD027636, 2017.

Yin, M. and Liu, G.: Assessment of GPM high-frequency microwave measurements with radiative transfer simulation under snowfall conditions, Q. J. R. Meteorol. Soc., 145(721), 1603–1616, doi:10.1002/qj.3515, 2019.

Yuter, S. E. and Houze, R. A.: Three-Dimensional Kinematic and Microphysical Evolution of Florida Cumulonimbus. Part II: Frequency Distributions of Vertical Velocity, Reflectivity, and Differential Reflectivity, Mon. Weather Rev., 123(7), 1941–1963, doi:10.1175/1520-0493(1995)123<1941:tdkame>2.0.co;2, 1995.

Zhang, J., Howard, K., Langston, C., Kaney, B., Qi, Y., Tang, L., Grams, H., Wang, Y., Cocks, S., Martinaitis, S., Arthur, A., Cooper, K., Brogden, J. and Kitzmiller, D.: Multi-Radar Multi-Sensor (MRMS) Quantitative Precipitation Estimation: Initial Operating Capabilities, Bull. Am. Meteorol. Soc., 97(4), 621–638, doi:10.1175/BAMS-D-14-00174.1, 2016.

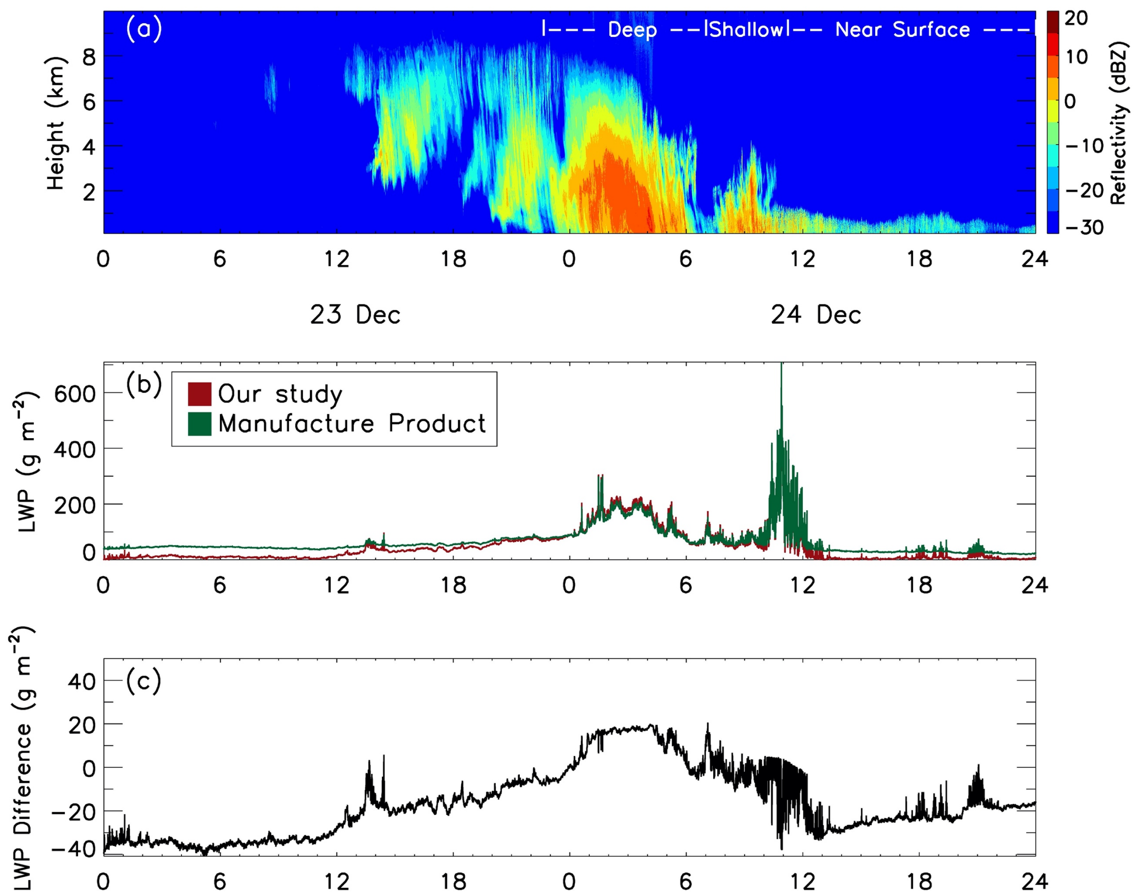

Fig.1 (a) Radar reflectivity, (b) two liquid water path retrievals and (c) their differences (LWP of our study plus manufacture product) for observations during 23 and 24 December 2017. In the top panel, cloud types as defined in the text are also indicated.

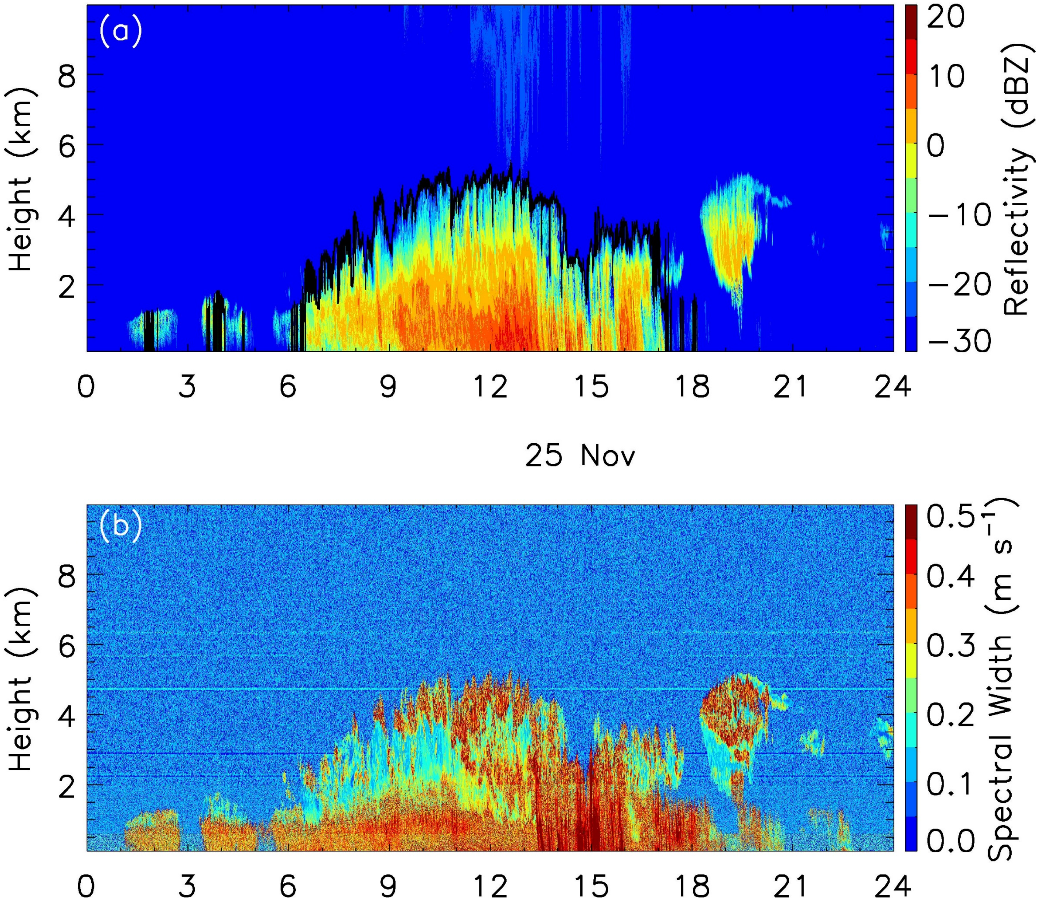

Fig.2 Height-time cross section of (a) radar reflectivity and (b) Doppler spectral width for observations on 25 November 2017. The cloud top for snowing clouds (surface radar reflectivity greater than -20 dBZ) is also shown in the top panel.

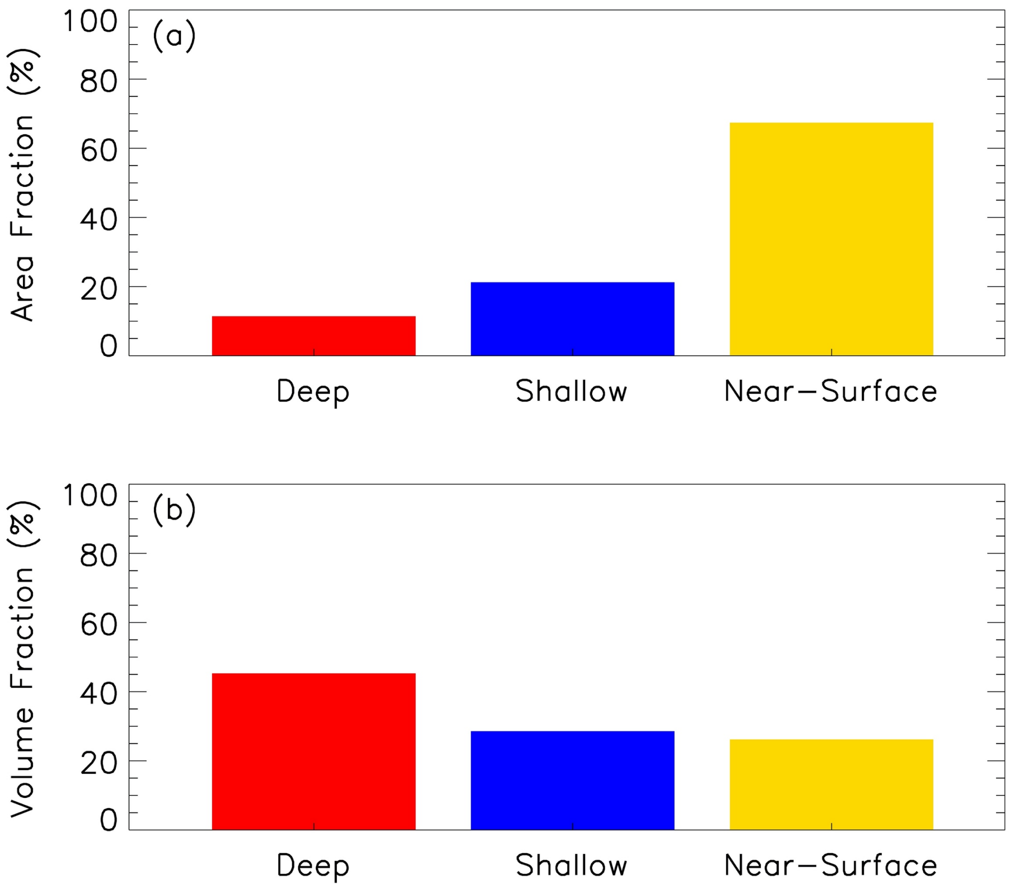

Fig.3 (a) Area and (b) volume fractions of the 3 types of snowing clouds observed during the 2017-18 winter season.

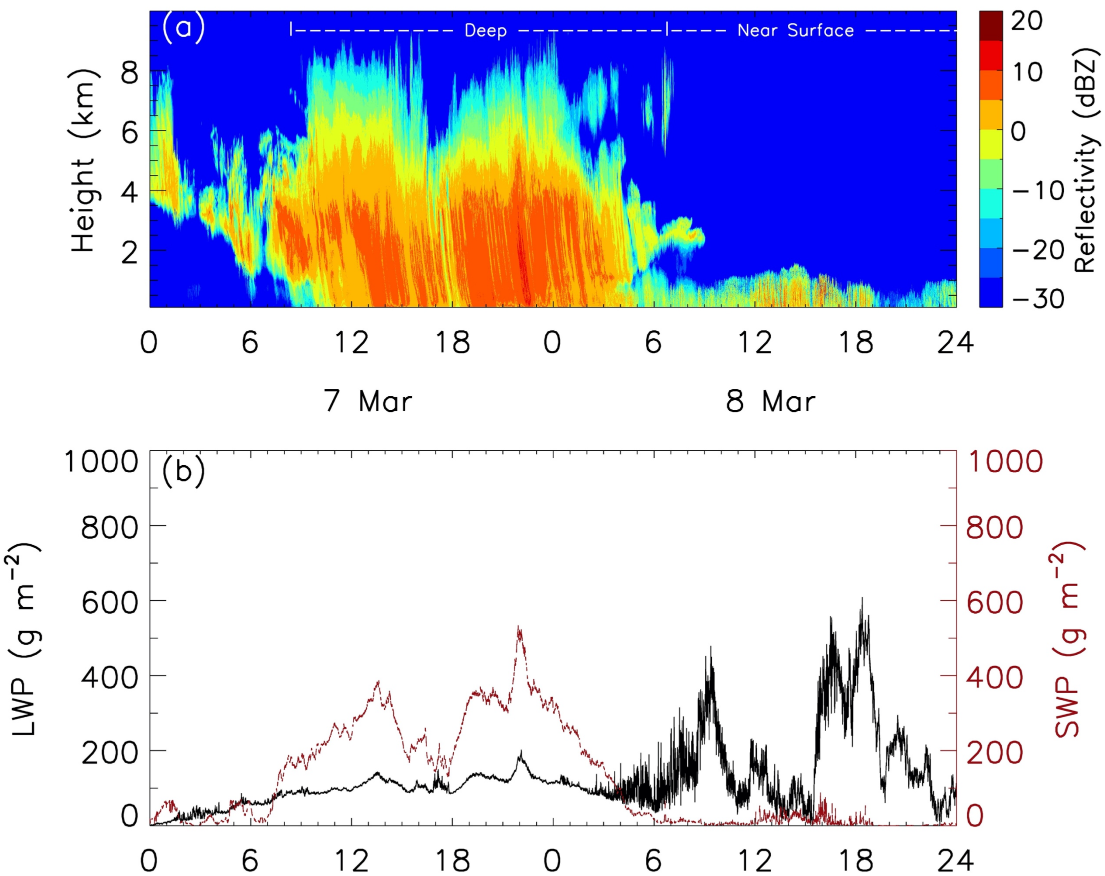

Fig.4 (a) Height-time cross section of radar reflectivity and (b) time series of liquid water path (LWP, black) and snow water path (SWP, red) for observations on 7 and 8 March 2018.

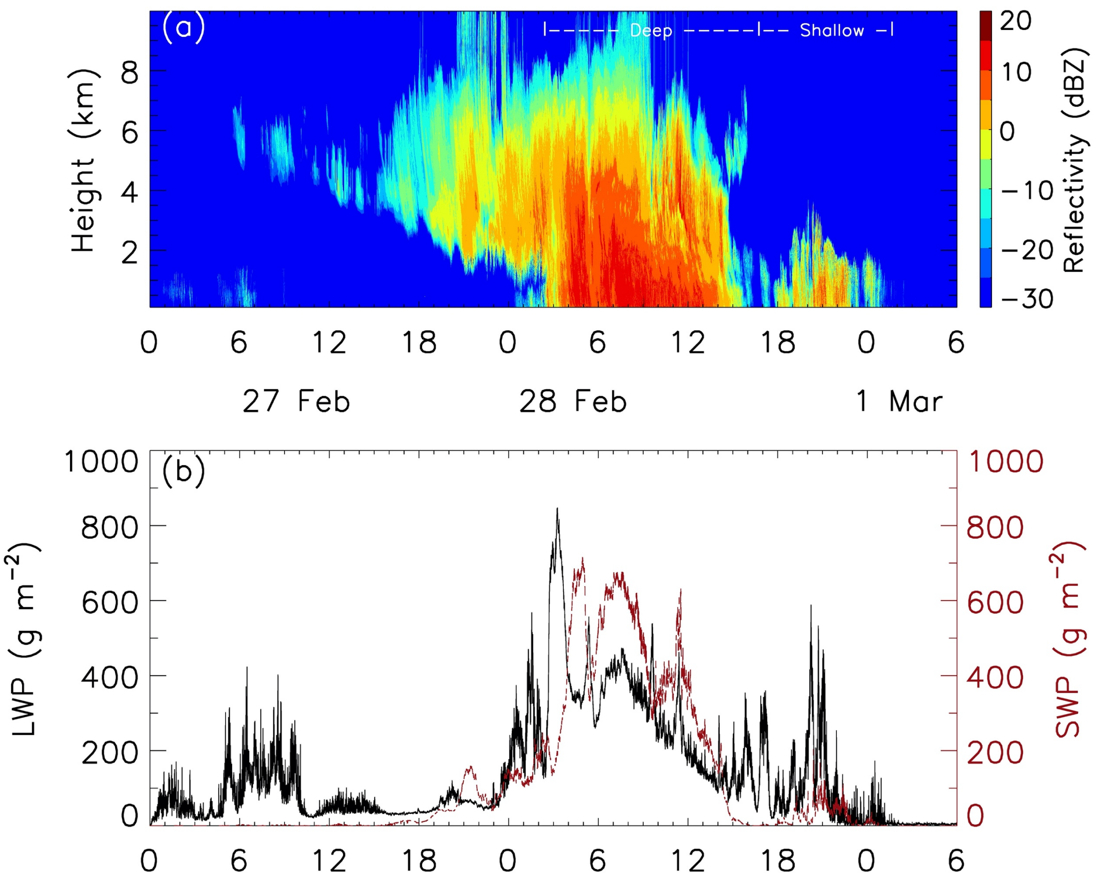

Fig.5 (a) Height-time cross section of radar reflectivity and (b) time series of liquid water path (LWP, black) and snow water path (SWP, red) for observations from 27 February through 1 March 2018.

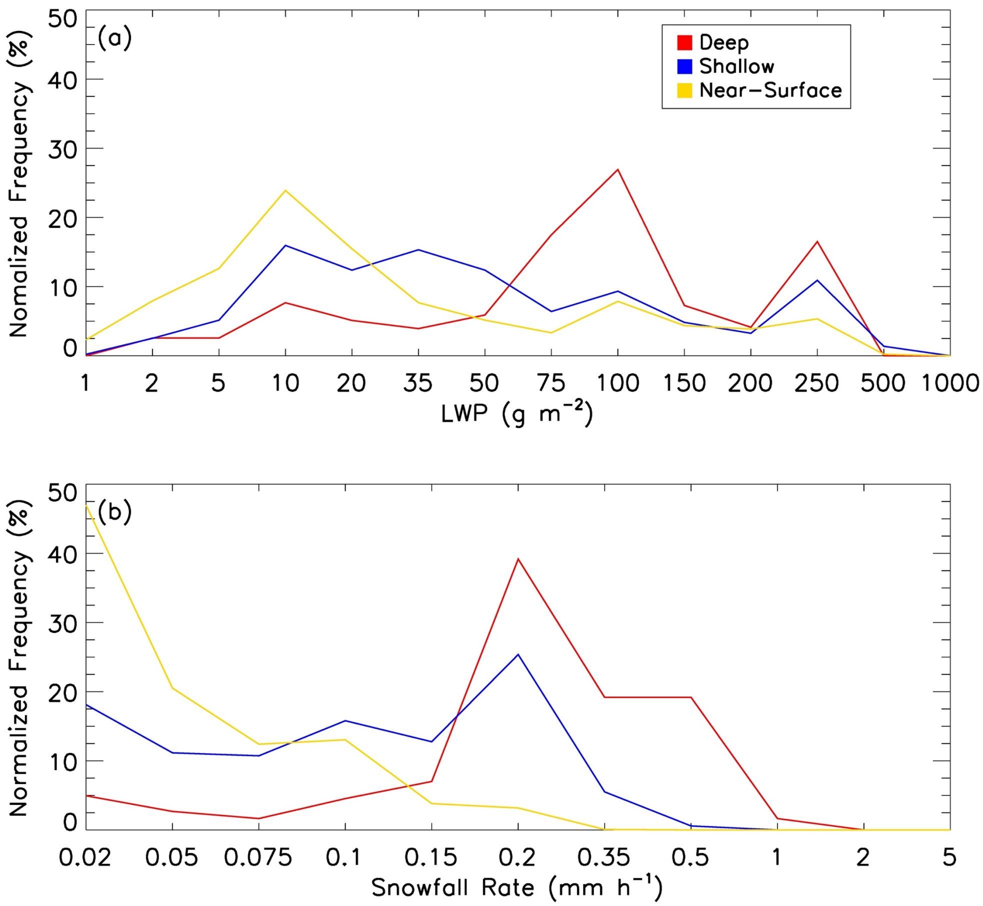

Fig.6 Frequency distribution of (a) liquid water path and (b) snowfall rate at surface derived from all observed snowfall data during the 2017-18 winter. The frequency values are normalized so that the sum of their values at all bins is 100%.

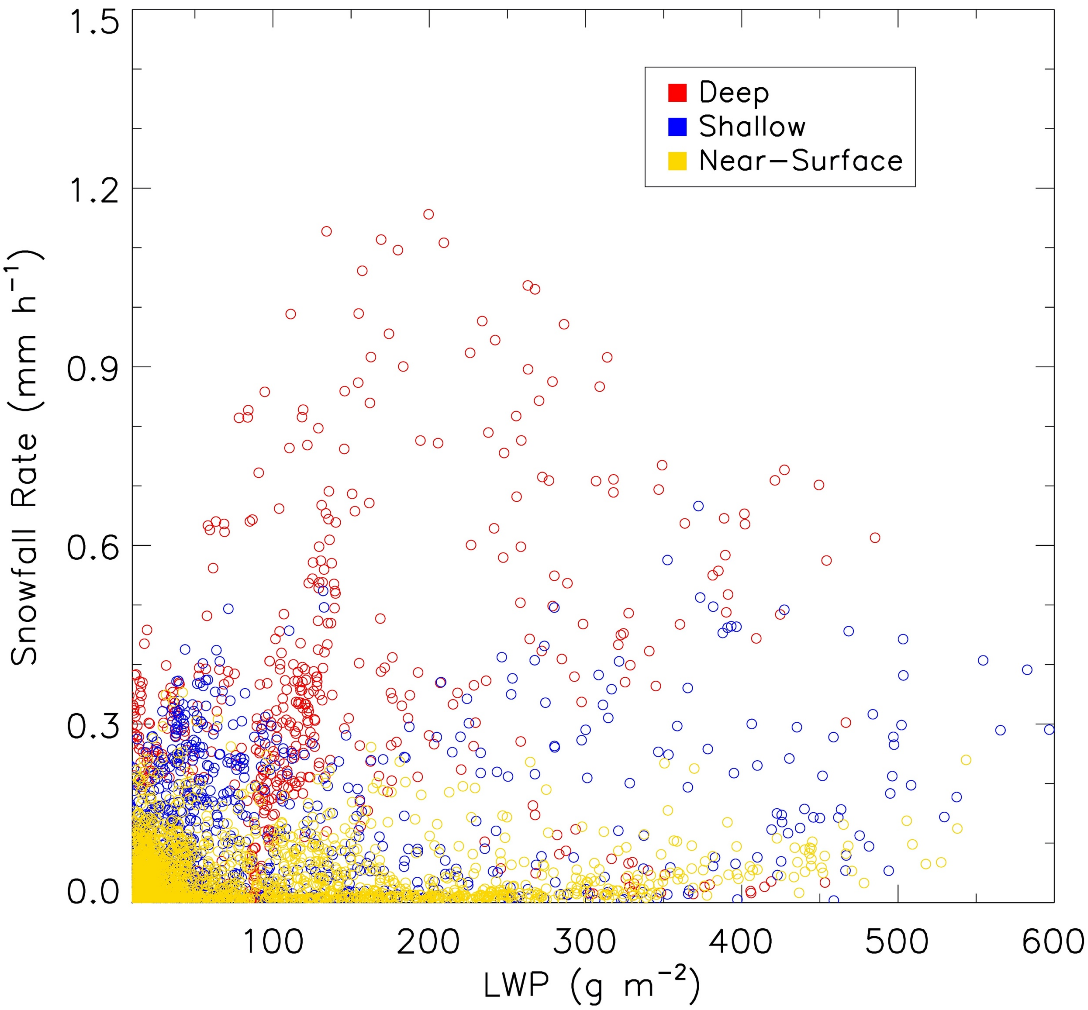

Fig.7 Scatterplot of liquid water path and surface snowfall rate. Each point is an average of 5-minute data. All observed data during the 2017-18 winter are included.

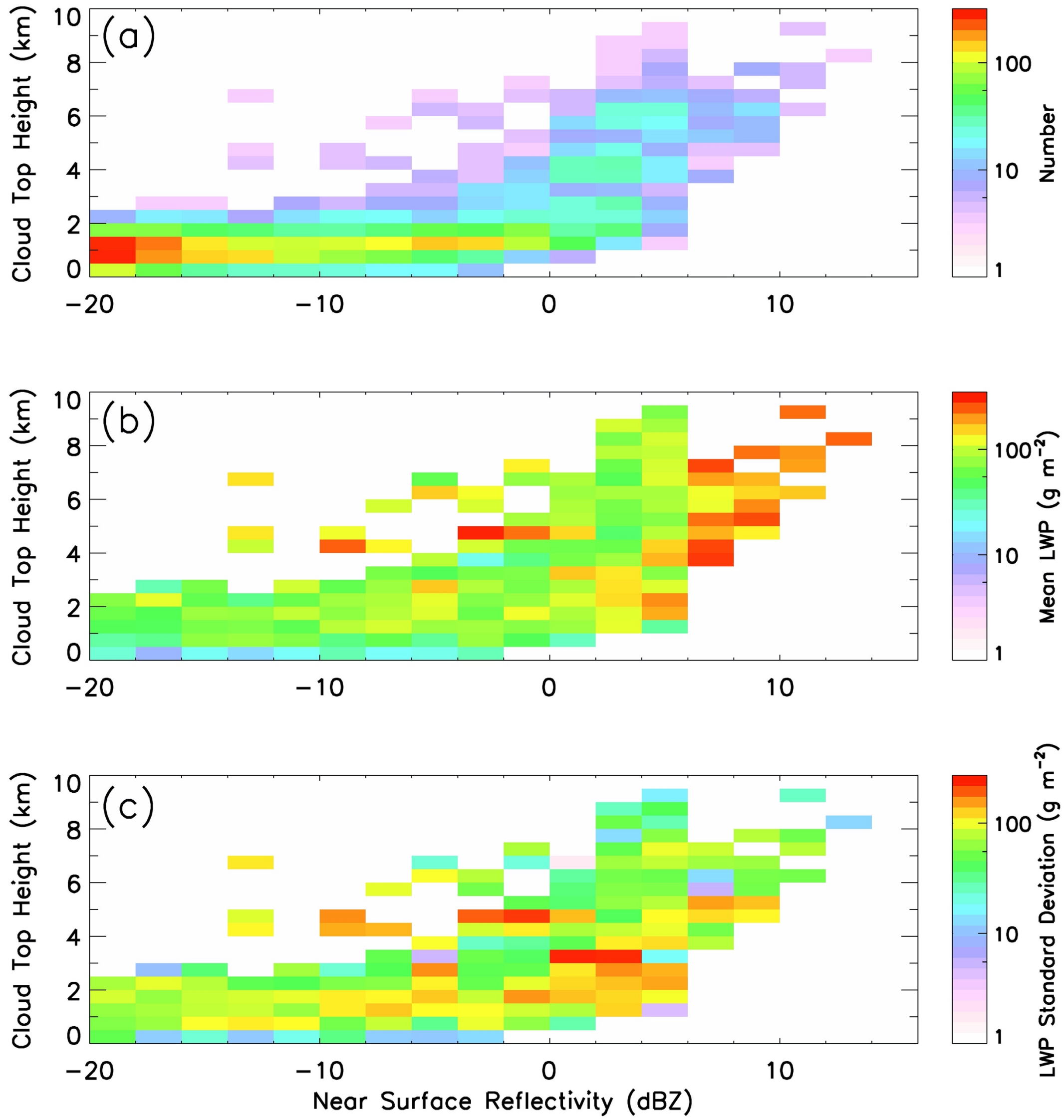

Fig.8 Two-dimensional distributions of (a) number of occurrences, (b) liquid water path and (c) standard deviation of liquid water path as a function of near surface radar reflectivity and cloud top height. All observed data during the 2017-18 winter are used in calculate the distributions.

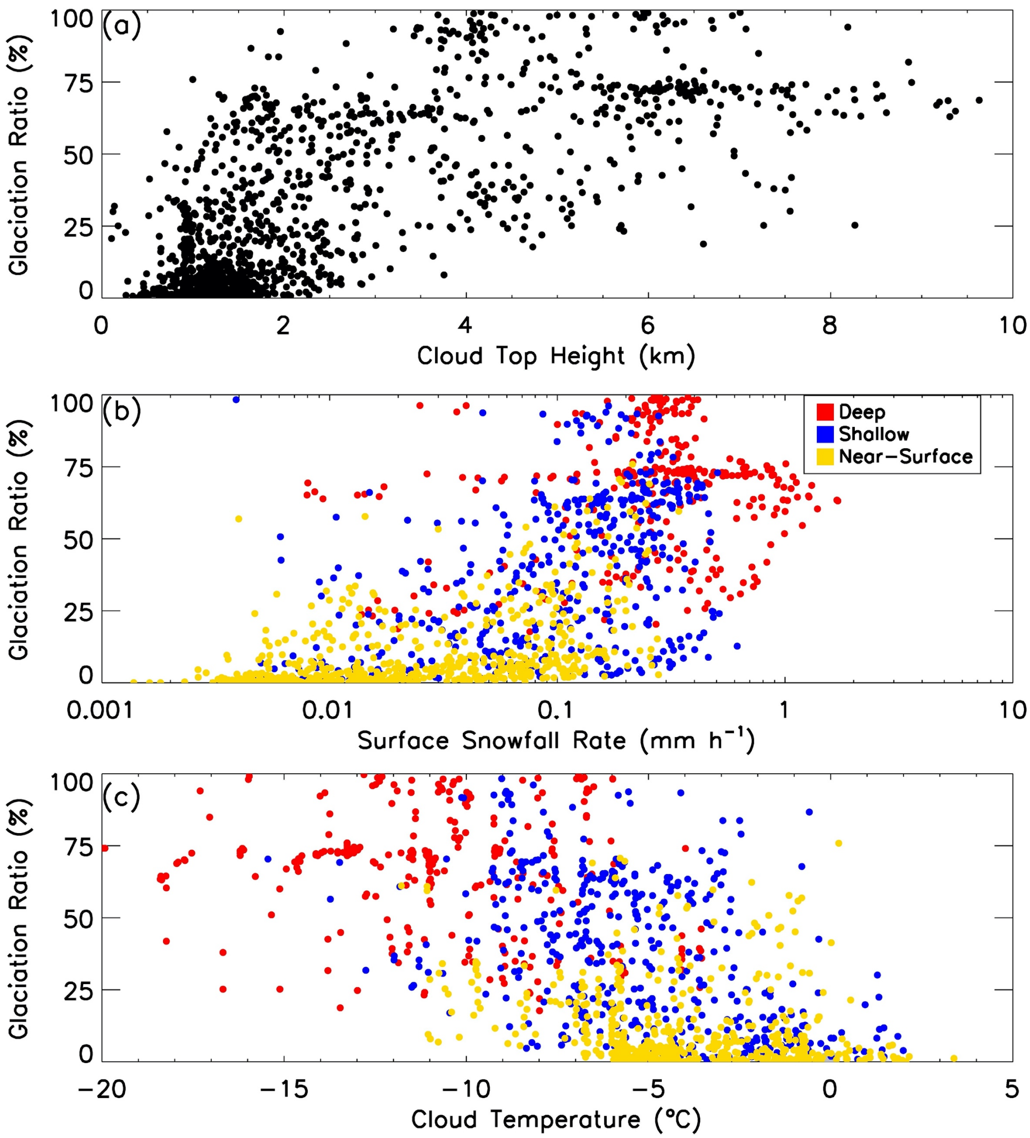

Fig.9 Scatterplot of glaciation ratio (see definition in the text) with (a) cloud top height, (b) surface snowfall rate and (c) cloud temperature based on 5-minute averages of all observational data of snowing clouds in the 2017-18 winter.

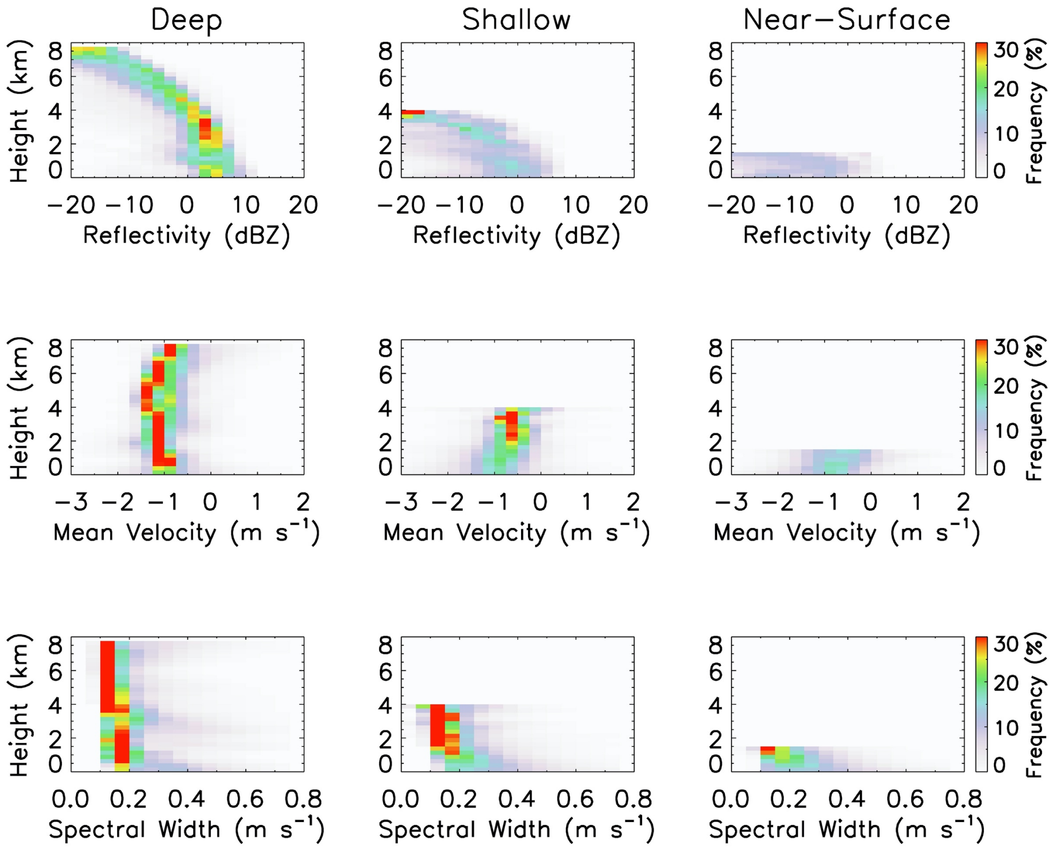

Fig.10 Contoured frequency by altitude diagram (CFADs) for radar reflectivity (top), mean Doppler velocity (middle) and Doppler spectral width (bottom) for deep (left), shallow (middle) and near-surface (right) snowing clouds. The frequency values are calculated in such a way that the sum of all frequency values at each altitude is 100%. All observed data from the 2017-18 winter are used.

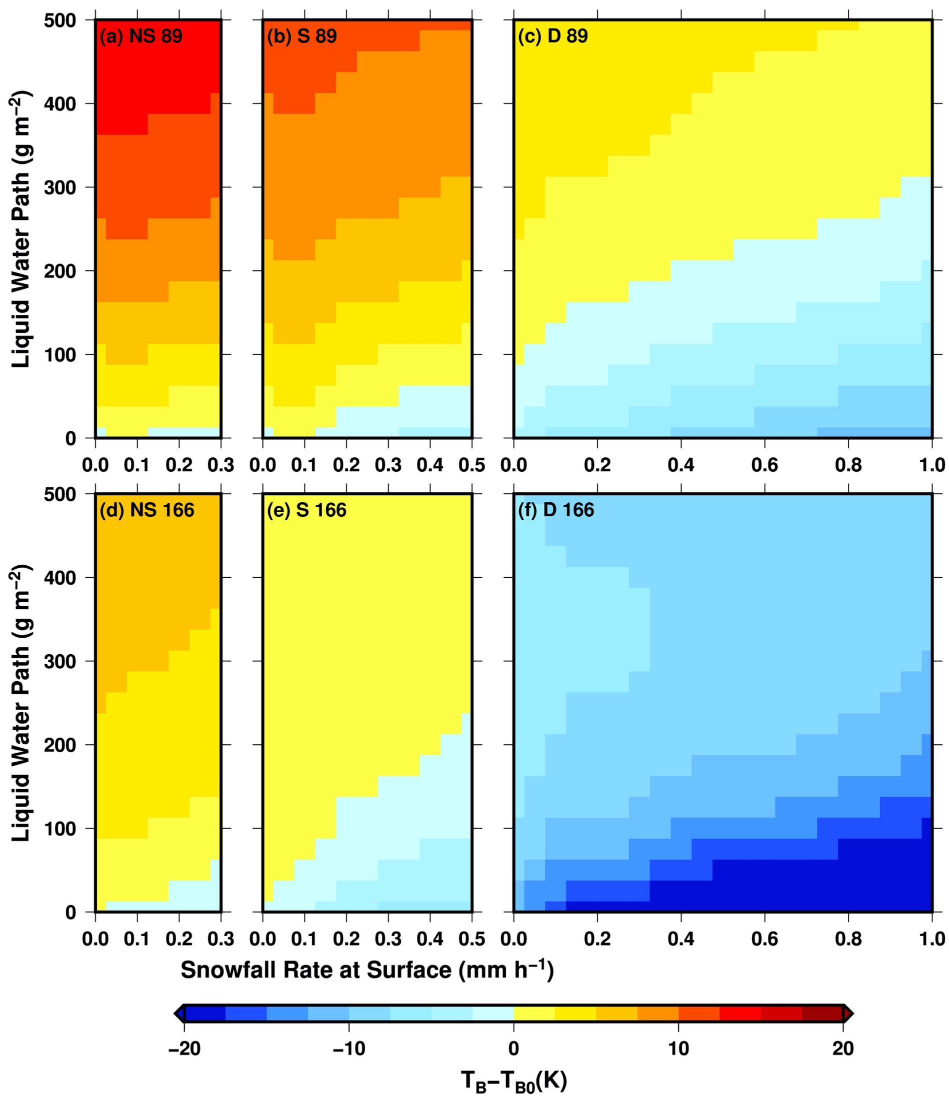

Fig.11 Simulated brightness temperature change (relative to clear-sky) at GMI 89 GHz (top) and 166 GHz (bottom) for near-surface (left), shallow (middle) and deep (right) snowing clouds. The change is relative to values at clear-sky.

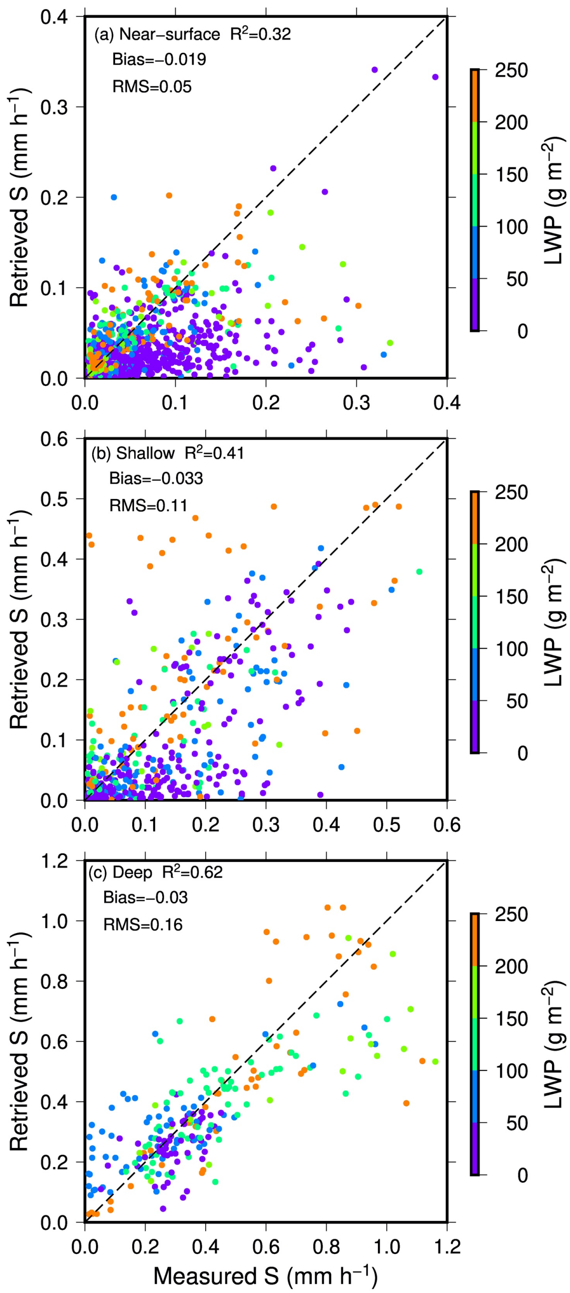

Fig.12 Scatterplot of "measured" versus "retrieved" snowfall rate for (a) near-surface, (b) shallow and (c) deep snowing clouds over land. Color of the points indicates liquid water path associated with the case. Correlation is indicated by R^2 in each diagram. Biases and root-mean-square (RMS) differences are also indicated in the diagrams.

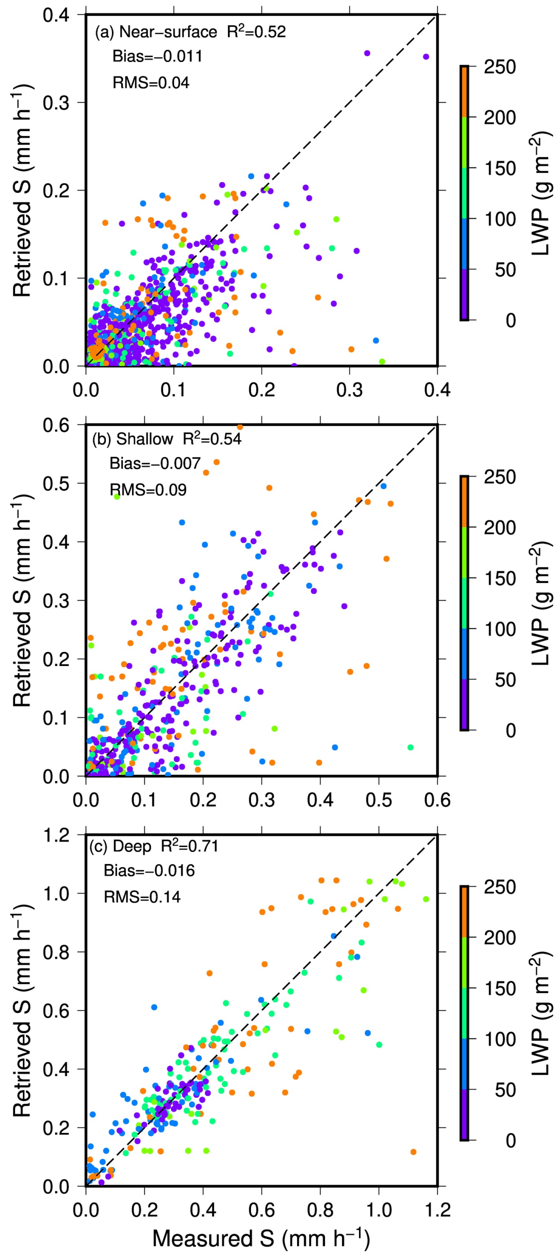

Fig.13 Scatterplot of "measured" versus "retrieved" snowfall rate for (a) near-surface, (b) shallow and (c) deep snowing clouds over ocean. Color of the points indicates liquid water path associated with the case. Correlation is indicated by R^2 in each diagram. Biases and root-mean-square (RMS) differences are also indicated in the diagrams.

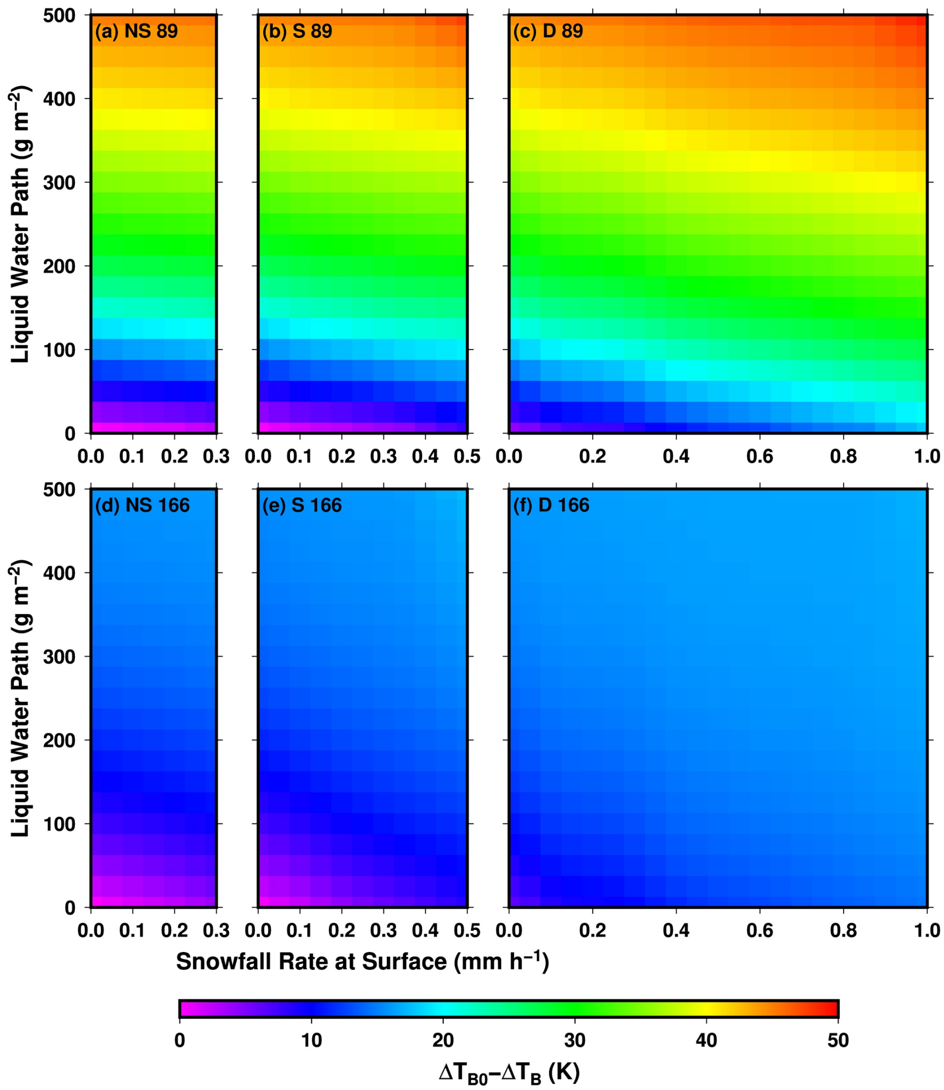

Fig.14 Simulated change of depolarization for GMI 89 GHz (top) and 166 GHz (bottom) for near-surface (left), shallow (middle) and deep (right) snowing clouds over ocean. Depolarization is the brightness temperature difference between vertical and horizontal polarizations. The change is relative to values at clear-sky.